Aus dem Institut für Lungenbiologie / Comprehensive Pneumology Center
des Helmholtz Zentrums München

Direktor: Prof. Dr. med. Oliver Eickelberg

Biodistribution von Gold-Nanopartikeln in Abhängigkeit von ihrer Größe, Oberflächenladung und Applikationsart

Dissertation

zum Erwerb des Doktorgrades der Humanbiologie

an der Medizinischen Fakultät der

Ludwig-Maximilians-Universität zu München

vorgelegt von

Stephanie Hirn

aus

Wertingen, Bayern, Deutschland

2013

Mit Genehmigung der Medizinischen Fakultät

der Universität München

Berichterstatter:	Prof. Dr. med. vet. Dr. med. habil. Fritz Krombach
Mitberichterstatter:	Prof. Dr. med. Alexander Baethmann
	Priv. Doz. Dr. med. Dirk-André Clevert
	Priv. Doz. Dr. med. Claus Neurohr
Dekan:	Prof. Dr. med. Dr. h.c. M. Reiser, FACR, FRCR
Tag der mündlichen Prüfung:	12.12.2013

Inhaltsverzeichnis

1 Einleitung

1.1 Nanopartikel

Die Vorsilbe „Nano" (nãnos = Zwerg) stammt aus dem Griechischen und impliziert bereits, dass es sich bei Nanopartikeln um sehr kleine Materialien handelt. Definitionsgemäß sind Nanopartikel in mindestens einer Raumdimension kleiner als 100 nm. Die Nanotechnologie gilt als eine der Schlüsseldisziplinen des 21. Jahrhunderts und wird, wie auch die Biotechnologie, als sogenannte Querschnittstechnologie angesehen, die in unterschiedlichen Anwendungsgebieten Verwendung finden kann. So werden verschiedenste Nanomaterialien z. B. in der Automobilindustrie, Energietechnik, Optik, Kosmetik, aber auch in der Medizin und Pharmaindustrie eingesetzt. Durch ihre geringen Ausmaße ist die Gesamtoberfläche von Nanopartikeln im Verhältnis zu ihrem Gesamtvolumen sehr viel größer als die der entsprechenden Ausgangsmaterialien (Abb. 1).

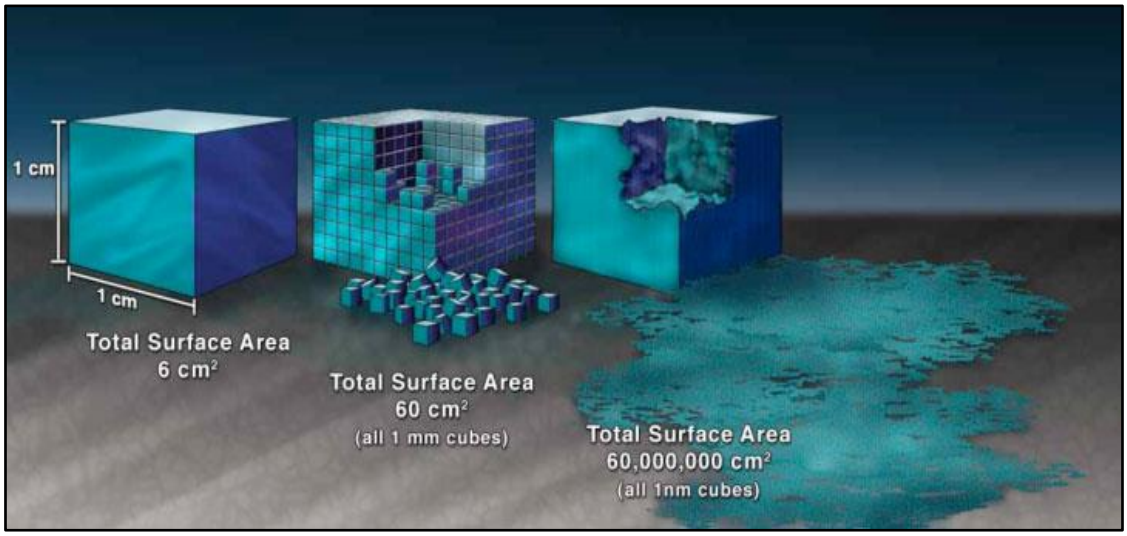

Abb. 1: Nanopartikel besitzen durch ein sehr viel größeres Oberflächen/Volumen-Verhältnis andere Eigenschaften als ihre Ausgangsmaterialien [1].

Daher ist auch die reaktive Oberfläche, mit welcher Nanopartikel mit ihrer Umgebung in Kontakt treten, weitaus größer. Zudem ergeben sich aus der geringen Größe veränderte physikalisch-chemische Eigenschaften wie beispielsweise eine bessere Leitfähigkeit, eine höhere Stabilität sowie eine herabgesetzte Schmelztemperatur.

Neben erwünschten Eigenschaften wie z. B. einem verbessertem UV-Schutz in Sonnencremes oder auch einer längeren Haltbarkeit von Lebensmitteln könnten diese neuen Materialien möglicherweise auch unerwünschte Eigenschaften wie z. B. eine kanzerogene oder auch DNA-schädigende Wirkung aufweisen und somit potentiell eine Gefährdung für Mensch und Umwelt darstellen. Entsprechende Übersichten über die Chancen und Risiken der Nanotechnologie können

beispielsweise den jeweiligen Internetauftritten des Bundesministeriums für Bildung und Forschung und des Bundes für Umwelt und Naturschutz auf ihren Homepages (www.bmbf.de/de/nanotechnologie.php; www.bund.net/themen_und_projekte/nanotechnologie/) entnommen werden.

Ein sehr vielversprechendes Feld der Nanotechnologie ist die Nanomedizin. Diese Disziplin umfasst sowohl die Erforschung neuer Methoden in der Diagnostik als auch die Entwicklung neuer Therapiemöglichkeiten. Gold-Nanopartikel scheinen hierfür besonders geeignet zu sein [2], worauf im folgenden Kapitel genauer eingegangen wird.

1.2 Gold-Nanopartikel

Gold-Nanopartikel wurden bereits 2.500 Jahre vor Chr. in Ägypten und China als Heilmittel oder für kosmetische Zwecke verwendet [3]. Im Mittelalter wurden beim Glasfärben unwissentlich Gold-Nanopartikel eingesetzt, wodurch Kirchenfenster ihre purpurrote Farbe erhielten. Aufgrund des Auftretens von Oberflächenplasmonenresonanz (SPR) variiert die Farbe von Gold-Nanopartikeln mit deren Größe (Abb. 2, links) und Form [4].

Hierbei führt die größenabhängige Resonanzschwingung der Elektronen zu einer größenspezifischen Lichtabsorption und somit erscheinen die betrachteten Gold-Nanopartikel je nach Größe in unterschiedlichen Farben. So zeigt sich auch ein Farbumschlag einer Gold-Nanopartikel-Suspension von Rot nach Blau, wenn eine Aggregatbildung stattfindet (Abb. 2, rechts).

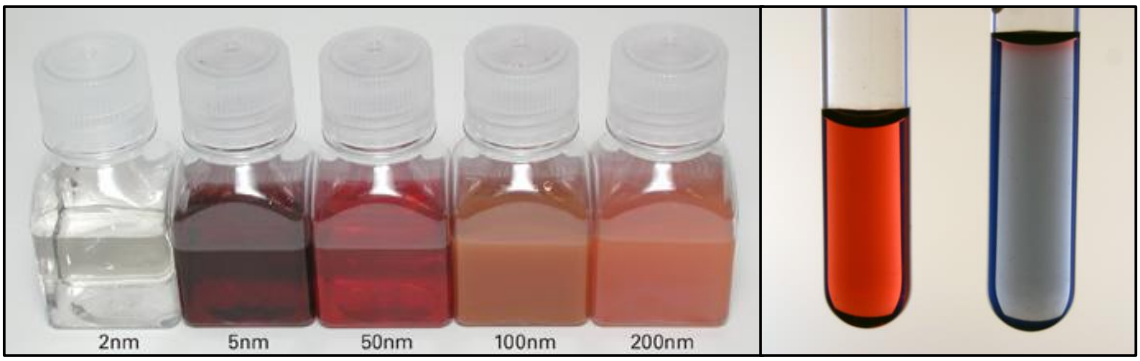

Abb. 2: links: Die Farbe von Gold-Nanopartikel-Suspensionen ist abhängig von der Partikelgröße [5]; rechts: Farbumschlag von Rot nach Blau bei Aggregatbildung der Gold-Nanopartikel [6]

1.2.1 Gold-Nanopartikel in der Nanomedizin

Für die medizinische Anwendung attraktiv sind Gold-Nanopartikel besonders wegen der Möglichkeit, durch relativ einfache Syntheseprozesse Liganden an ihre Oberfläche zu binden.
Dadurch kann u. a. eine zielgerichtete Aufnahme oder auch eine verlängerte Zirkulationszeit, die beispielsweise für eine passive Tumorakkumulation wichtig ist, bewirkt werden. Da Gold-Nanopartikel im Vergleich zu anderen metallischen Nanopartikeln nur eine geringe bzw. keine Toxizität zeigen [7], werden sie als vielsprechende Kandidaten für medizinische Anwendungen gesehen.
Gold-Nanopartikel werden z. B. für die Früherkennung von Infektionskrankheiten entwickelt. So versuchen Forscher Gold-Nanopartikel zur Detektion des Hepatitis-C-Virus als einfache und im Vergleich zu der herkömmlichen Methode kostengünstigere und schnellere Lösung zu nutzen [8]. Hierbei machen sich Azzazy *et al.* [9] den bereits in Kapitel 1.2 beschriebenen Farbumschlag bei der Aggregation von Gold-Nanopartikeln zu Nutze, indem eine stabile Gold-Nanopartikelsuspension aus dem Gleichgewicht gerät, wenn der zu testendende Erreger anwesend ist [9]. Eine weitere Detektionsmöglichkeit, wie sie z. B. bei Schwangerschaftstests [10] angewandt wird, ist die Anheftung bestimmter Antikörper an die Gold-Nanopartikel, die bei Anwesenheit des zu detektierenden Stoffes ihre typische rote bzw. blaue Färbung in einem Ergebnisfenster zeigen. Auch bakterielle Infektionen, wie z. B. die Salmonellose [11], können mit einem einfachen kolorimetrischen Test erkannt werden. Hierbei binden pink erscheinende Gold-Nanopartikel, die einen spezifischen Antikörper gebunden haben, an die Bakterien und ändern dadurch ihre Farbe nach Blau.
Außerdem werden Gold-Nanopartikel wegen ihrer photo-physikalischen Eigenschaften in Hinblick auf die Krebsfrüherkennung und auch zur (photothermalen) Therapie untersucht. Es gibt verschiedene Visualisierungsmöglichkeiten für die Darstellung von Gold-Nanopartikeln, die durch spezifische Marker an Tumorzellen binden; üblicherweise werden hierfür Oberflächen-Streuung, Zwei-Photonen-Fluoreszenz und oberflächenverstärkte Raman-Streuung genutzt [12,13].
Weiterhin gibt es bereits vielversprechende Forschungsergebnisse bezüglich des Einsatzes von Gold-Nanopartikeln als Röntgenkontrastmittel. So hat eine Studie zur Darstellung des vaskulären Systems in Mäusen gezeigt, dass die Visualisierung der applizierten Gold-Nanopartikel mit Röntgenmammographie um ein vielfaches besser ist als mit einem herkömmlich verwendeten iodinisierten Kontrastmittel [14].
Auch bei der Kombination von Ultraschall mit einer optischen Technik der sog. photoakustischen-photothermalen Bildgebung, zeigt sich mit Gold-Nanopartikeln eine verbesserte Visualisierung im Vergleich zu den ansonsten verwendeten organischen Farbstoffen [15].
In der photothermalen Therapie werden Agenzien benutzt, welche die Lichtenergie eines Lasers absorbieren und diese dann als Wärmestrahlung wieder abgeben. Dadurch kommt es im umliegenden Krebsgewebe zu einer Hyperthermie, welche die hitzeempfindlichen Tumorzellen zerstört [16]. Wie bereits in zahlreichen Studien untersucht wurde, besitzen auch Gold-Nanopartikel

diese Eigenschaft der Energieumwandlung [17]. Daher gibt es einige Untersuchungen, die sich mit dem Potential von Gold-Nanopartikeln für die photothermale Therapie beschäftigen. Hierbei akkumulierten die meist intravenös injizierten Gold-Nanopartikel im Tumor entweder durch passives oder aktives Tumortargeting und reduzierten bzw. stoppten dort ein weiteres Tumorwachstum [18-22]. Dabei scheint v. a. die Form der Nanopartikel eine entscheidende Rolle für den photothermalen Effekt zu spielen. So gibt es Untersuchungen zu länglich geformten Nanorods [23], eher rundlichen Nanoshells [24] oder hohlen Nanocages [25]. Hierbei zeigen die Nanorods einen stärkeren photothermalen Effekt als die anders geformten Gold-Nanopartikel. Sogenannte Nanostars weisen sogar eine noch höhere Energieumwandlung auf [26]. In der Zukunft wird die photothermale Therapie mit Gold-Nanopartikeln vermutlich in Kombination mit anderen Krebstherapien wie der Chemotherapie [27] oder der Strahlentherapie [24] zum Einsatz kommen.

Auch zur Strahlentherapie werden Gold-Nanopartikel verwendet, um die Zerstörung von Tumorzellen zu verstärken [28-30]. So zeigten Studien mit tumortragenden Mäusen bzw. Ratten, dass bei Verwendung von Gold-Nanopartikeln in Verbindung mit Strahlentherapie die Überlebensrate der Tiere durch die Reduzierung des Tumorgewebes stark anstieg, verglichen mit Tieren, die nur eine Bestrahlung ohne vorherige Gold-Nanopartikel-Gabe erhielten [31-33]. Häufig werden oberflächenmodifizierte Gold-Nanopartikel verwendet, um eine verbesserte Tumor-Akkumulation zu erzielen [34].

Bei der zielgerichteten Medikamentenapplikation (targeted drug delivery) unterscheidet man passive und aktive Formen. Im Tumorgewebe tritt der passive EPR- (erhöhter Permeabilitäts- und Retentions-) Effekt auf, der durch die gesteigerte Vaskularisierung und die erhöhte Durchlässigkeit der Blutgefäße [35] zu einer erhöhten Aufnahme von Nanopartikeln führen kann [18]. Allerdings ist der EPR-Effekt abhängig von der Dosis und auch von der Form der Nanopartikel [36].

Weiterhin kann ein aktives Tumortargeting durch die Bindung von tumorspezifischen Antikörpern an die Gold-Nanopartikel erreicht werden. Dadurch wird eine höhere Tumorakkumulation ermöglicht [37,38].

1.2.2 Toxizität von Gold-Nanopartikeln

Essentiell für die Verwendung von Gold-Nanopartikeln in der Nanomedizin ist die Einschätzung ihrer Toxizität. Einige Reviews fassen bereits die zahlreichen *in vitro* und *in vivo* Studien zusammen, bei denen entweder kein oder nur ein geringes toxisches Potential von Gold-Nanopartikeln nachgewiesen wurde [2,39-42]. In einigen Studien gibt es jedoch Hinweise auf einen geringfügigen Effekt, was die Hypothese nahelegt, dass die Toxizität nicht alleine von den Materialeigenschaften, sondern darüber hinaus von verschiedenen zusätzlichen Faktoren abhängig ist. So konnte *in vitro* nicht nur eine zelllinienabhängige Aufnahme [43], sondern auch eine zellspezifische Toxizität [44] gefunden werden. Aber auch die Größe der Nanopartikel scheint eine wichtige Rolle zu spielen, da Gold-Nanopartikel ≤ 20 nm im Vergleich zu nicht-toxischen größeren Partikeln *in vivo* einen gering toxischen Effekt zeigten [45]. Sehr kleine Gold-Nanopartikel mit einer

Größe von 1,4 nm im Durchmesser führten *in vitro*, vermutlich durch ihre größenbedingte Passgenauigkeit in die große Furche der DNA, zu zytotoxischen Effekten [46-48]. Des Weiteren zeigten Studien mit Gold-Nanopartikeln verschiedener Größen zwar eine Aufnahme in Zellen (K562 bzw. RAW 264.7) [49,50] bzw. ins Tumorgewebe [51] aber keine Toxizität.

Eine weitere wichtige Rolle spielt die Oberflächenmodifizierung der Gold-Nanopartikel. Daher wurde in Studien der Einfluss einer Oberflächenveränderung auf die Toxizität von Gold-Nanopartikeln untersucht. So zeigte sich *in vitro* trotz Aufnahme der oberflächenmodifizierten Partikel (mit Asparaginsäure, bovinem Serumalbumin oder Trinatriumcitrat-Dihydrat) kein zytotoxischer Effekt [49,52], wohingegen *in vivo* (Mausmodell) hepatotoxische und/oder nephrotoxische histologische Veränderungen gefunden wurden [52].

Als weiterer Faktor für die Toxizität von Nanopartikeln wird deren Morphologie diskutiert. So werden sphärische Gold-Nanopartikel von Zellen häufiger aufgenommen als Nanorods [53]. Allerdings konnte bisher noch kein Zusammenhang von Form und Toxizität von Gold-Nanopartikeln mit gleicher Oberflächenmodifikation und vergleichbarer Größe gefunden werden [54].

Eine Toxizitätsabschätzung von Nanopartikeln gestaltet sich oft schwierig, da teilweise nicht die Partikel selbst, sondern die zur Stabilisierung verwendete Hülle einen toxischen Effekt hervorrufen kann [39,55,56].

1.3 Pharmakokinetik

Die Pharmakokinetik oder auch Biokinetik befasst sich mit der Aufnahme, Verteilung, Metabolisierung und schließlich der Exkretion von Stoffen.

Dabei bestimmt bereits die Applikationsart entscheidend die nachfolgende Verteilung des Stoffes. Die intravasale Injektion bietet den Vorteil einer sehr schnellen Wirkung, da die Substanz sofort systemisch verfügbar ist. Die anwenderfreundliche orale Verabreichung eines Wirkstoffes kann einen First-Pass-Effekt nach sich ziehen. Dabei ist es möglich, dass der durch die Magen- bzw. Darmschleimhaut resorbierte Stoff mit dem Pfortaderblut als erstes in die Leber gelangt und dort zu einem Großteil metabolisiert und anschließend ausgeschieden wird. Diesem Effekt kann bis zu einem gewissen Grad mit einer erhöhten Dosierung entgegengewirkt werden, jedoch nicht unendlich, da aus manchen Pharmaka toxische Stoffwechselprodukte gebildet werden. Eine weitere wichtige Applikationsart stellt - insbesondere für die Therapie von Lungenerkrankungen - die Möglichkeit der Inhalation dar, wodurch das Medikament lokal zur Wirkung kommen kann. Da durch die Permeation eines Stoffes durch die Blut-Luft-Schranke die Substanz auch systemisch verfügbar wird, kann es im Anschluss zu einer Akkumulation in Sekundärorganen kommen (Abb. 3). Die physikalisch-chemischen Eigenschaften eines Stoffes sind von großer Bedeutung, da sie ent-scheidende Parameter für Aufnahme- oder Translokationsprozesse durch Membranen sind. So spielt einerseits die Polarität eine Rolle, aber auch die Molekülgröße ist relevant. Nur sehr kleine hydrophile Substanzen können transzellulär durch eine Membran treten, wobei größere Moleküle (>0,4 nm) eher parazellulär permeieren. Eine sehr dichte Barriere stellt die Blut-Hirn-Schranke dar,

da hier die Endothelzellen der Kapillaren über *tight junctions* verbunden und zusätzlich von einer enganliegenden Gliazellschicht ummantelt sind. Im Gegensatz dazu sind Lebersinusoide mit einer diskontinuierlicher Membran (0,1 – 0,5 µm) ausgekleidet, die einen einfacheren Flüssigkeits- bzw. Stoffdurchtritt erlaubt. Interessanterweise gibt es einige Studien, die feststellen, dass Nanopartikel auch relativ undurchlässige Membranen überwinden können [57].

Weiterhin spielt in der Pharmakokinetik die Exkretion eines Stoffes eine entscheidende Rolle. Man unterscheidet zwischen der renalen und biliären Ausscheidung. Letztere bezeichnet den Stofftransport über Gallengänge in den Dünndarm. Allerdings hängen die Exkretionswege von Substanzen stark von deren physikalisch-chemischen Eigenschaften ab.

Im Folgenden wird auf die Biokinetik mit Fokus auf die Biodistribution von Gold-Nanopartikeln näher eingegangen.

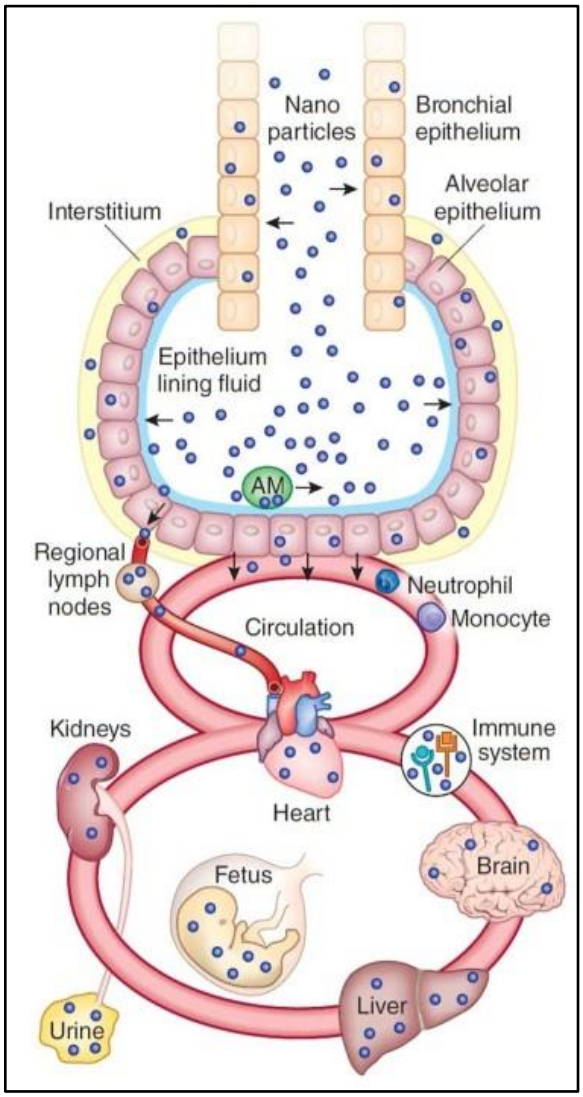

Abb. 3: Biodistribution von Nanopartikeln im Körper nach Inhalation [58]

1.4 Biokinetik von Gold-Nanopartikeln

Mit Hinblick auf die medizinische Anwendbarkeit von Nanopartikeln sind Studien zur Biokinetik essentiell.

In biokinetischen Studien werden verschiedene Messmethoden verwendet, die unterschiedliche Vor- und Nachteile aufweisen. Eine sehr häufig angewandte Methode ist die Massenspektrometrie mit induktiv gekoppeltem Plasma (ICP-MS). Hierbei wird die flüssige Probe mittels Argon-Plasma bei Temperaturen von 5.000 – 10.000°C ionisiert und anschließend in einem Massenspektrometer analysiert. Die spezifischen Elementmassen ermöglichen eine qualitative und quantitative Differenzierung mit einer Genauigkeit von 0,001 – 0,1 µg/l. Somit findet die Messtechnik der ICP-MS auch Anwendung zur Quantifizierung von Gold-Nanopartikeln in Geweben, Blut oder Urin [59-61]. Daneben stellen die Atomemissions-Spektroskopie (AES) [62] und die Atomabsorptions-Spektrometrie (AAS) [63] verwandte Formen der Massenspektrometrie dar, wobei beide Methoden auf der Lichtabsorption der Probe beruhen. Allerdings werden bei diesen Methoden nur geringe Mengen einer Organprobe analysiert. Anschließend werden die Messergebnisse auf das gesamte Organvolumen extrapoliert. Dies kann bei einer heterogenen Nanopartikeldeposition im Organ zu einer Über- bzw. Unterbewertung der tatsächlichen Nanopartikelakkumulation führen.

Präzisere Messergebnisse können mit dem Einsatz von Radioaktivität erreicht werden, da durch die Bestrahlung und somit Aktivierung von (Gold-)Nanopartikeln die Nachweisgrenze (ca. 0,1 Bq [64]) herabgesetzt werden kann und eine Messung kompletter Organe möglich ist. Anstatt der Neutronen- bzw. Protonenaktivierung der Gold-Nanopartikel ist auch eine Anheftung von radioaktiven Markern an die Partikeloberfläche möglich [65]. Dieses Verfahren birgt jedoch die Gefahr einer Ablösung des radioaktiven Isotops, was zu einer Fehlinterpretation der Ergebnisse führen kann und somit zusätzliche Untersuchungen erfordert.

Bei der Verwendung von radioaktiven (Gold-)Partikeln werden quantitative und qualitative bildgebende Verfahren unterschieden. Radioaktive Gold-Nanopartikel können mittels Gammakamera, Computertomographie (CT) [66] bzw. Einzelphotonen-Emissionscomputertomographie (SPECT) [67] oder Positronen-Emissions-Tomographie (PET) [68] dargestellt werden. Für quantitative Messungen gibt es die Möglichkeit der Gammaspektroskopie [69], bei der radioaktive Gold-Nanopartikel appliziert werden und anschließend die Gammaemission der zu untersuchenden Organe gemessen wird. Hierbei können auch nicht-radioaktive Gold-Nanopartikel verwendet werden. Bei dieser Methode wird die zu untersuchende Probe erst im Nachhinein bestrahlt. Anschließend kann der Goldgehalt der Probe mit Hilfe von Neutronenaktivierungsanalyse (INAA) [70,71] bestimmt werden.

Diese eben beschriebenen Methoden werden für Untersuchungen zur Biodistribution von Gold-Nanopartikeln eingesetzt. Bisher gibt es bereits einige Studien, in denen die *in vivo* Biodistribution nach intravenöser Injektion von Gold-Nanopartikeln unterschiedlicher physikalischer Eigenschaften untersucht wurde. Hierbei wurde hauptsächlich der Einfluss von Größe, Form und Oberflächenmodifikation analysiert. So zeigt sich nach intravenöser Gabe eine größenabhängige

Ausscheidungsrate über den Urin, wobei kleinere Gold-Nanopartikel den Körper schneller verlassen [14,51] als größere. Außerdem ist die Akkumulation von Gold-Nanopartikeln in der Leber mit einer Größe über 5 nm höher als die von kleineren Partikeln [51,59,70,72]. Aber auch die Ladung von (Gold-)Nanopartikeln scheint deren Verteilungsmuster zu beeinflussen. So zeigten Untersuchungen mit Dendrimeren, die 2 nm Gold-Nanopartikeln beinhalten, je nach Ladung eine unterschiedliche Verteilung. Hierbei war die Akkumulation von positiv geladenen Dendrimeren in der Niere am höchsten, wohingegen die negativ geladenen und neutralen Dendrimere am häufigsten in der Leber gefunden wurden [70].

Weiterhin spielt die Form der Gold-Nanopartikel eine wichtige Rolle für die Verteilung im Körper. In einer Studie zeigten längliche Gold-Nanorods im Vergleich zu sphärischen Gold-Nanopartikeln eine längere Blut-Halbwertszeit und eine höhere Leberakkumulation [54].

Allerdings scheint vor allem die sogenannte Proteinkorona [73], eine Biomolekülhülle, die sich um Nanopartikel bildet (Abb. 4), sobald ein Partikel mit einer biologischen Flüssigkeit in Kontakt tritt, für die Verteilungsmuster verantwortlich zu sein. Die Proteinkorona wird als instabile Anlagerung von Biomolekülen vermutet, die dynamischen Prozessen unterworfen ist und sich somit je nach Milieu verändern kann [74].

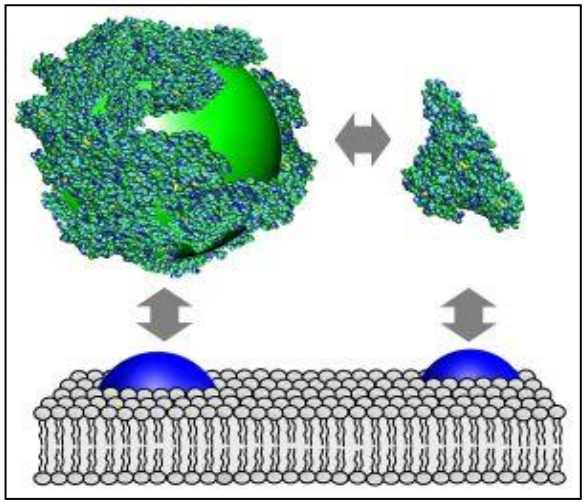

Abb. 4: Proteine (grün-blau), die an der Zellmembran z. B. an Rezeptoren (blau) binden, umgeben Nanopartikel (grün), was zur Interaktion der Nanopartikel mit der Zellmembran führt [75].

Dieser Aspekt kann auch für die biomedizinische Anwendungen von Vorteil sein. So wird die Oberfläche von Nanopartikeln häufig mit Polyethylenglycol (PEG) [76,77] modifiziert, um eine lange Blutzirkulation und verminderte Aufnahme der (Gold-)Nanopartikel durch das MPS (Mononukleäre Phagozytensystem) zu erreichen [78]. Des Weiteren konnte auch durch eine Oberflächenmodifikation mit Glutathion [79] die Zirkulationszeit der Gold-Nanopartikel verlängert werden.

In *in vitro* Studien wurde bereits gezeigt, dass die Größe von Gold-Nanopartikel einen Einfluss auf die Anheftung von Proteinen an deren Oberfläche hat, was dann wiederum zu unterschiedlich starker zellulärer Aufnahme dieser Partikel führte [43].

Allgemein ist allerdings zu erwähnen, dass die meisten Biodistributionsstudien nicht die gesamte biokinetische Verteilung untersuchen und üblicherweise nur einen Fokus auf ausgewählte Organe legen. Weiterhin werden meistens nur die Verteilungen der Gold-Nanopartikel nach intravenöser oder intraperitonealer Injektion betrachtet, andere Applikationsrouten wie z. B. Inhalation oder orale Medikamentenapplikation bleiben aber weitgehend unbeachtet. Daher war das Ziel der vorliegenden Arbeiten eine zu 100% quantitative Biodistribution von Gold-Nanopartikeln in Abhängigkeit von Größe, Oberflächenladung und Applikationsart wiederzugeben.

2 Zusammenfassung

Gold-Nanopartikel besitzen vielfältige und vielversprechende Möglichkeiten in der Nanomedizin in Bezug auf Imaging, Diagnostik und Therapie. Da bisher nur ein begrenztes Wissen über das *in vivo* Verhalten von Gold-Nanopartikeln existiert, ist es notwendig, deren Biokinetik grundlegend zu betrachten. Bisher gibt es noch keine Untersuchung, welche die gesamte Bioverteilung von Gold-Nanopartikeln betrachtet. So wurde in den beiden vorliegenden Studien jeweils eine zu hundert Prozent quantitativ ausbalancierte Biodistribution von Gold-Nanopartikeln erhoben, um ein unverzerrtes Verteilungsbild zu erhalten. Dabei wurde der Einfluss der Größe und der Oberflächenladung auf die Biodistribution von Gold-Nanopartikeln nach Applikation mittels intravenöser Injektion oder oraler Gabe untersucht. Die intravenöse Injektion dient in der Medizin als einer der Hauptapplikationswege, da das Medikament auf diese Weise direkt in die Blutzirkulation gelangt und im ganzen Körper verteilt wird. Demgegenüber steht die orale Gabe, die sich vor allem durch ihre Anwenderfreundlichkeit auszeichnet.

Um einen möglichen Zusammenhang zwischen der Biodistribution von Gold-Nanopartikeln und deren Größe bzw. Oberflächenladung zu bestimmen, wurden radioaktive Gold-Nanopartikel in sechs verschiedenen Größen (1,4 nm, 2,8 nm, 5 nm, 18 nm, 80 nm, 200 nm; die 2,8 nm Gold-Nanopartikel hatten entweder eine positive oder negative Oberflächenladung) weiblichen Ratten entweder intravenös oder intra-oesophageal unter Narkose verabreicht. Anschließend wurden die Tiere 24 h nach Applikation euthanasiert und die Verteilung der Gold-Nanopartikel im gesamten Körper sowie bereits ausgeschiedene Gold-Nanopartikel zu 100% mit Hilfe von gamma-spektrometrischen Messungen bestimmt.

Nach intravenöser Injektion retinierte der Hauptanteil der Gold-Nanopartikel aller untersuchten Größen und Ladungen in der Leber (51,3 – 96,9%). Weiterhin war die Leberakkumulation von Gold-Nanopartikeln ≤ 5 nm linear abhängig von der volumenspezifischen Oberfläche (VSSA; 1/nm) (Abb. 5, links). Auch für die anderen Organe (Niere, Herz, Gehirn, Uterus) sowie den Restkörper, Blut und Urin war die Gold-Nanopartikel-Akkumulation linear abhängig von der VSSA für Gold-Nanopartikel-Größen von 1,4 nm bis 5 nm. In anderen Worten, die kleinsten Gold-Nanopartikel akkumulierten in Niere, Herz, Gehirn, Uterus sowie in Restkörper, Blut und Urin häufiger als die größeren Partikel. Ab einer Größe von 18 nm zeigten die Gold-Nanopartikel weder eine größenabhängige Verteilung noch eine größenabhängige renale Exkretion. Interessanterweise verlief die hepatobiliäre Exkretion der Gold-Nanopartikel ≥ 2,8 nm linear zu ihrem Durchmesser - umso kleiner die Partikel, umso größer deren biliäre Exkretion.

Außerdem wurde eine ladungsabhängige Verteilung der 2,8 nm Gold-Nanopartikel festgestellt. Die negativ geladenen Partikel retinierten stärker in der Leber, wohingegen in allen anderen Organen die positiv geladenen Partikel häufiger akkumulierten.

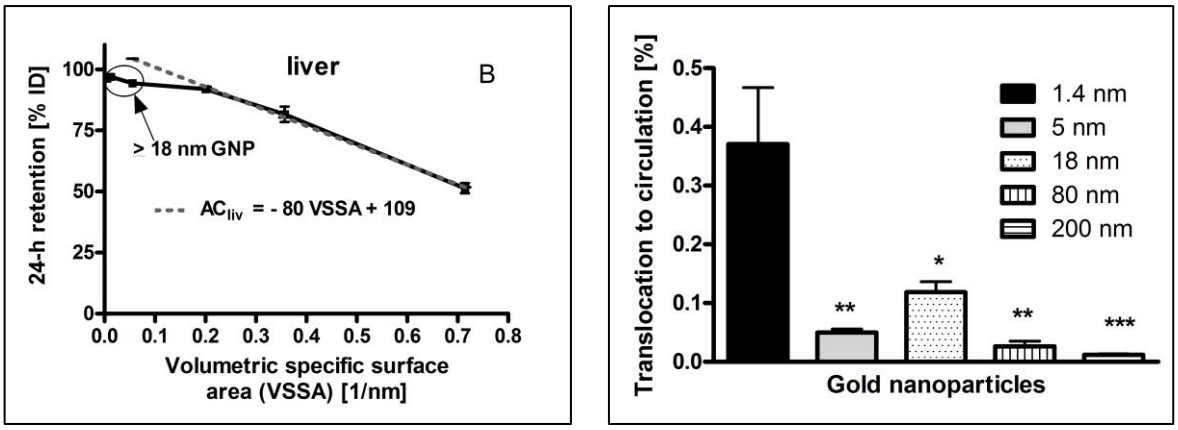

Abb. 5: links: Abhängigkeit der Leberakkumulation von der volumenspezifischen Oberfläche (VSSA) [80]; rechts: Gesamttranslokation der Gold-Nanopartikel durch die Darmschranke in die Zirkulation [81]

Nach oraler Applikation retinierte, wie zu erwarten, die Mehrzahl der Gold-Nanopartikel, unabhängig von Ladung und Größe im Gastro-Intestinal-Trakt bzw. war bereits mit dem Kot ausgeschieden worden. Allerdings durchquerte auch ein kleiner Prozentsatz der applizierten Partikel (Abb. 5, rechts) in Abhängigkeit von ihrer Größe die Darmschranke, wobei die kleinsten Gold-Nanopartikel (1,4 nm) mit Abstand am stärksten translozierten. Erstaunlicherweise nehmen die 18 nm kleinen Partikel eine Sonderrolle ein, da sie mit 0,12% um einen Faktor 2 häufiger die Blutzirkulation erreichten als die kleineren 5 nm Gold-Nanopartikel. Weiterhin zeigten die 18 nm Gold-Nanopartikel auch im Blut, im Restkörper, im Herz und auch im Gehirn eine stärkere Akkumulation als die kleineren 5 nm Partikel, für die letzten beiden Organe sogar einen höheren Anteil als für die kleinsten, 1,4 nm Gold-Nanopartikel.

Weiterhin konnte auch für die 2,8 nm Partikel eine Abhängigkeit der Akkumulation von der Oberflächenladung festgestellt werden. Der Anteil der durch die Darmschranke in die Blutzirkulation übergetretenen Gold-Nanopartikel war für die negativ geladenen 2,8 nm Gold-Nanopartikel signifikant höher als für die positiv geladenen. So wurden die negativ geladenen Partikel in der Leber, dem Restkörper und auch im Urin signifikant mehr retiniert bzw. ausgeschieden. Außerdem akkumulierten nur die positiv geladenen, nicht aber die negativ geladenen Partikel, zu einem geringen Anteil im Gehirn.

Der große Vorteil der beiden vorliegenden Studien liegt in der Gesamtheit der Datenerhebung. So sind hierbei nicht nur einzelne Organe eines Organismus auf ihren Gold-Nanopartikel-Gehalt untersucht worden, sondern es wurden alle Organe, Körperbestandteile und zusätzlich alle Ausscheidungen berücksichtigt. Es zeigte sich nicht nur eine starke Akkumulation der Gold-Nanopartikel in der Leber, sondern auch eine vergleichsweise hohe Gold-Nanopartikel-Akkumulation im Restkörper, bestehend aus Skelett, Muskulatur, Fettgewebe und Haut (Fell), die in anderen Studien zur Biodistribution vernachlässigt werden. Weiterhin konnte durch die Verwendung von radioaktiven Gold-Nanopartikeln eine hohe Detektionsrate erreicht werden. Dies

ermöglichte die Verwendung einer kleinen Applikationsmenge, die keine toxischen Effekte erwarten lässt, aber trotzdem den Nachweis von sehr geringen Mengen (z. B. im Gehirn) erlaubt.
Zusammenfassend zeigen diese Studien eine größen- und oberflächenladungsabhängige Biodistribution von Gold-Nanopartikeln. Betrachtet man die beiden Studienergebnisse, zeigt sich weiterhin, dass der Aufnahmeweg einen entscheidenden Einfluss auf die Biodistribution von Gold-Nanopartikeln hat.

3 Summary

Gold nanoparticles are auspicious candidates in nanomedicine for imaging, diagnostics, and therapy. At present, only a limited understanding of the *in vivo* properties of gold nanoparticles exists, however. Therefore, it is mandatory to study the biodistribution of gold nanoparticles. Currently, there are no published studies which have considered the complete mass-balance for the biodistribution of gold nanoparticles. Consequently, in the two present studies a one hundred percent balanced quantitative biodistribution of gold nanoparticles was measured, in order to provide an unbiased assessment of the distribution pattern. The influence of size and surface modification on the biodistribution of gold nanoparticles following intravenous injection or oral application was measured. In medicine, intravenous injection is one of the most common application routes, allowing the administered drug to directly enter the systemic circulation and to distribute throughout the whole body. In contrast, the oral route is characterized by a more user-friendly and less invasive application.

Therefore, in order to observe a possible correlation between biodistribution and size or surface-charge of gold nanoparticles, we have administered radioactive gold nanoparticles of six different sizes (1.4 nm, 2.8 nm, 5 nm, 18 nm, 80 nm, 200 nm; the 2.8 nm gold nanoparticles having either a positive or a negative surface charge) to anesthetized female rats intravenously or intra-esophageally. The animals were sacrificed 24 h post exposure. Then, a 100% biodistribution of the applied gold nanoparticles was quantitatively measured by gamma-spectrometry.

After intravenous injection, the majority of gold nanoparticles of all sizes and charges accumulated in the liver (51.3 – 96.9%). Furthermore, the retention of gold nanoparticles ≤ 5 nm in the liver was linearly dependent on the volumetric specific surface area (VSSA; 1/nm). Hence, the accumulation of gold nanoparticles increased with decreasing VSSA (Abb. 6, left). Also in all the other organs (kidneys, heart, brain, and uterus) as well as in the remaining carcass (consisting of skin, skeleton, and soft tissue), blood, and urine, the accumulation of gold nanoparticle sizes between 1.4 and 5 nm was linearly dependent on the VSSA. In other words, the smallest gold nanoparticles accumulated in kidneys, heart, brain, and uterus as well as in the remaining carcass, blood, and urine to a higher extent than the bigger particles. Gold nanoparticles ≥ 18 nm displayed neither a size-dependent biodistribution nor a size-dependent renal excretion pattern. Interestingly, the hepato-biliary clearance of gold nanoparticles ≥ 2.8 nm was linearly dependent on their particle diameter; the smaller the particles, the higher the hepato-biliary excretion.

Moreover, a charge-dependent distribution of the 2.8 nm gold nanoparticles occurred. There was a higher retention in liver of the negatively charged particles, while in all other organs the negatively charged particles accumulated less than the positively charged particles.

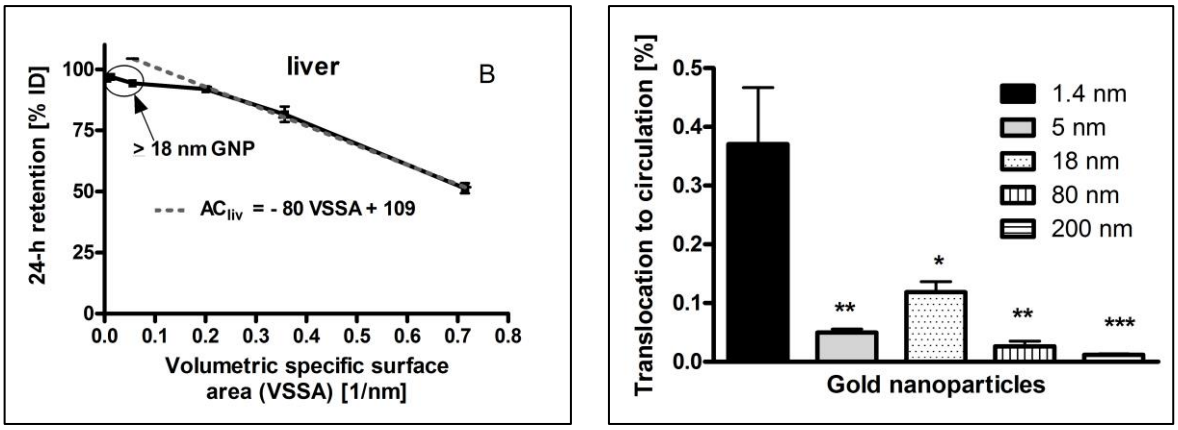

Figure 1 left: The liver accumulation is dependent on the volumetric specific surface area (VSSA) [80]; right: Total gold nanoparticle translocation through the intestinal barrier into the circulation [81]

As expected after oral application, the majority of gold nanoparticles, independent of size and surface charge, remained in the gastro-intestinal tract or were excreted within feces. However, a small percentage of the administered particles (Abb. 6, right) also crossed the intestinal barrier, the smallest gold nanoparticles (1.4 nm) showing by far the highest translocation. Surprisingly, the 18 nm gold nanoparticles showed an anomalous response, as they reached the blood circulation with 0.12% efficiency, about ten times higher than the smaller 5 nm particles. Furthermore, the 18 nm gold nanoparticles accumulated to a greater extent than the smaller 5 nm particles in the blood, in the remaining body, in heart, and also in brain. Additionally, the smallest 1.4 nm particles were retained to a lesser extent than the 18 nm gold nanoparticles in the heart and brain.

Moreover, a surface charge-dependent accumulation of the 2.8 nm gold nanoparticles was also determined. Negatively charged 2.8 nm particles crossed through the intestinal barrier into the blood circulation in significantly higher amounts than positively charged 2.8 nm particles. As a result, more negatively charged particles were detected in the liver, remaining body, and urine. In the brain however, only the positively charged particles but not the negatively charged gold nanoparticles accumulated to a small extent.

The great advantage of the two present studies lies in the completeness of data acquisition. In this regard, not only single organs have been chosen for examination, but all organs, the remaining body, and additionally all excretions from the animal were considered. Hence, there was not only a high accumulation of gold nanoparticles in the liver, but also a comparatively high gold nanoparticle retention in the remaining body, consisting of skeleton, muscles, skin (fur), and adipose tissue. This information has been neglected in most other studies. Furthermore, through the use of radioactive gold nanoparticles, a high detection rate was achieved. This allowed the usage of low administration doses with no acute toxicity to any of the organs. Nonetheless, it was possible to measure small amounts of gold nanoparticles (*e.g.* in brain).

Taken together, these two studies indicate a size- and surface charge-dependent biodistribution of gold nanoparticles. Furthermore, the route of administration appears to be crucial for the resultant biodistribution of gold nanoparticles.

4 Abbildungsverzeichnis

5 Literaturverzeichnis

1 National Nanotechnology Initiative, What's So special about the Nanoscale? http://www.nano.gov/nanotech-101/special (Stand: 19.03.2013).

2 Panyala, N. R., Pena-Mendez, E. M. & Havel, J. Gold and nano-gold in medicine: overview, toxicology and perspectives. *J Appl Biomed* (2009) **7**, 75-91.

3 Daniel, M. C. & Astruc, D. Gold nanoparticles: Assembly, supramolecular chemistry, quantum-size-related properties, and applications toward biology, catalysis, and nanotechnology. *Chem Rev* (2004) **104**, 293-346.

4 Mie, G. Beiträge zur Optik trüber Medien, speziell kolloidaler Metallösungen. *Ann. Phys.* (1908) **5**, 377-445.

5 Ted Pella Inc., Gold colloids. http://www.tedpella.com/gold_html/goldsols.htm (Stand: 15.03.2013).

6 Lisensky, G. Quantum Dots & Nanoparticles. http://mrsec.wisc.edu/Edetc/background/quantum_dots/index.html (Stand: 19.03.2013).

7 Lewinski, N., Colvin, V. & Drezek, R. Cytotoxicity of nanoparticles. *Small* (2008) **4**, 26-49.

8 Zohny, H. Nanoscale gold to help diagnose HCV infection 2011 http://www.nature.com/nmiddleeast/2011/110304/full/nmiddleeast.2011.27.html (Stand 19.03.2013).

9 Shawky, S. M., Bald, D. & Azzazy, H. M. Direct detection of unamplified hepatitis C virus RNA using unmodified gold nanoparticles. *Clinical biochemistry* (2010) **43**, 1163-1168.

10 Heckmann, J. Schwangerschaftstests 2006. http://www.pta-aktuell.de/media/pdf/2006/Oktober_06/PTA_10_Intern_040_048.pdf (Stand 19.03.2013).

11 Wang, S. *et al.* Rapid colorimetric identification and targeted photothermal lysis of Salmonella bacteria by using bioconjugated oval-shaped gold nanoparticles. *Chemistry* (2010) **16**, 5600-5606.

12 Huang, X., Jain, P. K., El-Sayed, I. H. & El-Sayed, M. A. Gold nanoparticles: interesting optical properties and recent applications in cancer diagnostics and therapy. *Nanomedicine (Lond)* (2007) **2**, 681-693.

13 Larguinho, M. & Baptista, P. V. Gold and silver nanoparticles for clinical diagnostics - From genomics to proteomics. *J Proteomics* (2012) **75**, 2811-2823.

14 Hainfeld, J. F., Slatkin, D. N., Focella, T. M. & Smilowitz, H. M. Gold nanoparticles: a new X-ray contrast agent. *Br J Radiol* (2006) **79**, 248-253.

15 Li, W., Brown, P. K., Wang, L. V. & Xia, Y. Gold nanocages as contrast agents for photoacoustic imaging. *Contrast media & molecular imaging* (2011) **6**, 370-377.

16 Rhee, J. G., Eddy, H. A., Harrison, G. H. & Salazar, O. M. Heat-sensitive state of mouse mammary carcinoma cells in tumors. *Radiat Res* (1990) **123**, 165-170.

17 Huang, X., Jain, P. K., El-Sayed, I. H. & El-Sayed, M. A. Plasmonic photothermal therapy (PPTT) using gold nanoparticles. *Lasers in medical science* (2008) **23**, 217-228.

18 Hamad, I. & Moghimi, S. M. Critical issues in site-specific targeting of solid tumours: the carrier, the tumour barriers and the bioavailable drug. *Expert Opin Drug Deliv* (2008) **5**, 205-219.

19 Dreaden, E. C., Alkilany, A. M., Huang, X., Murphy, C. J. & El-Sayed, M. A. The golden age: gold nanoparticles for biomedicine. *Chem Soc Rev* (2012) **41**, 2740-2779.

20 Choi, W. I. *et al.* Tumor regression in vivo by photothermal therapy based on gold-nanorod-loaded, functional nanocarriers. *ACS Nano* (2011) **5**, 1995-2003.

21 Ungureanu, C. *et al.* Light interactions with gold nanorods and cells: implications for photothermal nanotherapeutics. *Nano Lett* (2011) **11**, 1887-1894.

22 Kennedy, L. C. *et al.* A new era for cancer treatment: gold-nanoparticle-mediated thermal therapies. *Small* (2011) **7**, 169-183.

23 Samim, M., Prashant, C. K., Dinda, A. K., Maitra, A. N. & Arora, I. Synthesis and characterization of gold nanorods and their application for photothermal cell damage. *International Journal of Nanomedicine* (2011) **6**, 1825-1831.

24 Atkinson, R. L. *et al.* Thermal enhancement with optically activated gold nanoshells sensitizes breast cancer stem cells to radiation therapy. *Science translational medicine* (2010) **2**, 55ra79.

25 Cobley, C. M., Au, L., Chen, J. & Xia, Y. Targeting gold nanocages to cancer cells for photothermal destruction and drug delivery. *Expert Opin Drug Deliv* (2010) **7**, 577-587.

26 Yuan, H. *et al.* In vivo particle tracking and photothermal ablation using plasmon-resonant gold nanostars. *Nanomedicine* (2012) **8**, 1355-1363.

27 You, J. *et al.* Photothermal-chemotherapy with doxorubicin-loaded hollow gold nanospheres: A platform for near-infrared light-trigged drug release. *Journal of controlled release : official journal of the Controlled Release Society* (2012) **158**, 319-328.

28 Gannon, C. J., Patra, C. R., Bhattacharya, R., Mukherjee, P. & Curley, S. A. Intracellular gold nanoparticles enhance non-invasive radiofrequency thermal destruction of human gastrointestinal cancer cells. *J Nanobiotechnology* (2008) **6**, 2.

29 Kong, T. *et al.* Enhancement of radiation cytotoxicity in breast-cancer cells by localized attachment of gold nanoparticles. *Small* (2008) **4**, 1537-1543.

30 Rahman, W. N. *et al.* Enhancement of radiation effects by gold nanoparticles for superficial radiation therapy. *Nanomedicine* (2009) **5**, 136-142.

31 Elsherbini, A. A., Saber, M., Aggag, M., El-Shahawy, A. & Shokier, H. A. Laser and radiofrequency-induced hyperthermia treatment via gold-coated magnetic nanocomposites. *International journal of nanomedicine* (2011) **6**, 2155-2165.

32 Hainfeld, J. F., Slatkin, D. N. & Smilowitz, H. M. The use of gold nanoparticles to enhance radiotherapy in mice. *Phys Med Biol* (2004) **49**, N309-N315.

33 Hainfeld, J. F., Smilowitz, H. M., O'Connor, M. J., Dilmanian, F. A. & Slatkin, D. N. Gold nanoparticle imaging and radiotherapy of brain tumors in mice. *Nanomedicine (Lond)* (2012), Epub ahead of print.

34 Zhang, X. D. *et al.* Size-dependent radiosensitization of PEG-coated gold nanoparticles for cancer radiation therapy. *Biomaterials* (2012) **33**, 6408-6419.

35 Maeda, H., Fang, J., Inutsuka, T. & Kitamoto, Y. Vascular permeability enhancement in solid tumor: various factors, mechanisms involved and its implications. *International immunopharmacology* (2003) **3**, 319-328.

36 Puvanakrishnan, P., Park, J., Chatterjee, D., Krishnan, S. & Tunnell, J. W. In vivo tumor targeting of gold nanoparticles: effect of particle type and dosing strategy. *International journal of nanomedicine* (2012) **7**, 1251-1258.

37 Arvizo, R. R. *et al.* Identifying new therapeutic targets via modulation of protein corona formation by engineered nanoparticles. *PloS one* (2012) **7**, e33650.

38 Chattopadhyay, N. *et al.* Design and characterization of HER-2-targeted gold nanoparticles for enhanced X-radiation treatment of locally advanced breast cancer. *Molecular pharmaceutics* (2010) **7**, 2194-2206.

39 Alkilany, A. M. & Murphy, C. J. Toxicity and cellular uptake of gold nanoparticles: what we have learned so far? *Journal of nanoparticle research : an interdisciplinary forum for nanoscale science and technology* (2010) **12**, 2313-2333.

40 Boisselier, E. & Astruc, D. Gold nanoparticles in nanomedicine: preparations, imaging, diagnostics, therapies and toxicity. *Chem Soc Rev* (2009) **38**, 1759-1782.

41 Johnston, H. J. *et al.* A review of the in vivo and in vitro toxicity of silver and gold particulates: particle attributes and biological mechanisms responsible for the observed toxicity. *Crit Rev Toxicol* (2010) **40**, 328-346.

42 Khlebtsov, N. & Dykman, L. Biodistribution and toxicity of engineered gold nanoparticles: a review of in vitro and in vivo studies. *Chem Soc Rev* (2011) **40**, 1647-1671.

43 Chithrani, B. D. & Chan, W. C. Elucidating the mechanism of cellular uptake and removal of protein-coated gold nanoparticles of different sizes and shapes. *Nano Lett* (2007) **7**, 1542-1550.

44 Patra, H. K., Banerjee, S., Chaudhuri, U., Lahiri, P. & Dasgupta, A. K. Cell selective response to gold nanoparticles. *Nanomedicine* (2007) **3**, 111-119.

45 Abdelhalim, M. A. Gold nanoparticles administration induces disarray of heart muscle, hemorrhagic, chronic inflammatory cells infiltrated by small lymphocytes, cytoplasmic vacuolization and congested and dilated blood vessels. *Lipids in health and disease* (2011) **10**, 233.

46 Liu, Y. *et al.* Gold-cluster degradation by the transition of B-DNA into A-DNA and the formation of nanowires. *Angew Chem Int Ed Engl* (2003) **42**, 2853-2857.

47 Pan, Y. *et al.* Size-dependent cytotoxicity of gold nanoparticles. *Small* (2007) **3**, 1941-1949.

48 Pan, Y. *et al.* Gold nanoparticles of diameter 1.4 nm trigger necrosis by oxidative stress and mitochondrial damage. *Small* (2009) **5**, 2067-2076.

49 Connor, E. E., Mwamuka, J., Gole, A., Murphy, C. J. & Wyatt, M. D. Gold nanoparticles are taken up by human cells but do not cause acute cytotoxicity. *Small* (2005) **1**, 325-327.

50 Zhang, Q., Hitchins, V. M., Schrand, A. M., Hussain, S. M. & Goering, P. L. Uptake of gold nanoparticles in murine macrophage cells without cytotoxicity or production of pro-inflammatory mediators. *Nanotoxicology* (2011) **5**, 284-295.

51 Glazer, E. S. *et al.* Biodistribution and acute toxicity of naked gold nanoparticles in a rabbit hepatic tumor model. *Nanotoxicology* (2011) **5**, 459-468.

52 Das, S., Debnath, N., Mitra, S., Datta, A. & Goswami, A. Comparative analysis of stability and toxicity profile of three differently capped gold nanoparticles for biomedical usage. *Biometals : an international journal on the role of metal ions in biology, biochemistry, and medicine* (2012) **25**, 1009-1022.

53 Chithrani, B. D., Ghazani, A. A. & Chan, W. C. Determining the size and shape dependence of gold nanoparticle uptake into mammalian cells. *Nano Lett* (2006) **6**, 662-668.

54 Arnida, Alexander, M. & Hamidreza, G. Cellular uptake and toxicity of gold nanoparticles in prostate cancer cells: a comparative study of rods and spheres. *Journal of Applied Toxicology* (2010) **30**, 212-217.

55 Qiu, Y. *et al.* Surface chemistry and aspect ratio mediated cellular uptake of Au nanorods. *Biomaterials* (2010) **31**, 7606-7619.

56 Rivera-Gil, P. *et al.* The Challenge To Relate the Physicochemical Properties of Colloidal Nanoparticles to Their Cytotoxicity. *Accounts of chemical research* (2012), Epub ahead of print.

57 Pietroiusti, A., Campagnolo, L. & Fadeel, B. Interactions of Engineered Nanoparticles with Organs Protected by Internal Biological Barriers. *Small* (2012), Epub ahead of print.

58 Kreyling, W. G., Hirn, S. & Schleh, C. Nanoparticles in the lung. *Nat Biotechnol* (2010) **28**, 1275-1276.

59 De Jong, W. H. *et al.* Particle size-dependent organ distribution of gold nanoparticles after intravenous administration. *Biomaterials* (2008) **29**, 1912-1919.

60 Sadauskas, E. *et al.* Biodistribution of gold nanoparticles in mouse lung following intratracheal instillation. *Chem Cent J* (2009) **3**, 16.

61 Sonavane, G., Tomoda, K. & Makino, K. Biodistribution of colloidal gold nanoparticles after intravenous administration: effect of particle size. *Colloids and surfaces. B, Biointerfaces* (2008) **66**, 274-280.

62 Goel, R., Shah, N., Visaria, R., Paciotti, G. F. & Bischof, J. C. Biodistribution of TNF-alpha-coated gold nanoparticles in an in vivo model system. *Nanomedicine (Lond)* (2009) **4**, 401-410.

63 Terentyuk, G. S. *et al.* Circulation and distribution of gold nanoparticles and induced alterations of tissue morphology at intravenous particle delivery. *J Biophotonics* (2009) **2**, 292-302.

64 Kreyling, W. G., Semmler-Behnke, M., Takenaka, S. & Moller, W. Differences in the Biokinetics of Inhaled Nano- versus Micrometer-Sized Particles. *Accounts of chemical research* (2012), Epub ahead of print.

65 Hebert, E. M., Debouttiere, P. J., Lepage, M., Sanche, L. & Hunting, D. J. Preferential tumour accumulation of gold nanoparticles, visualised by Magnetic Resonance Imaging: radiosensitisation studies in vivo and in vitro. *International journal of radiation biology* (2010) **86**, 692-700.

66 Wen, S. *et al.* Multifunctional dendrimer-entrapped gold nanoparticles for dual mode CT/MR imaging applications. *Biomaterials* (2013) **34**, 1570-1580.

67 Ocampo-Garcia, B. E. *et al.* (99m)Tc-labelled gold nanoparticles capped with HYNIC-peptide/mannose for sentinel lymph node detection. *Nuclear medicine and biology* (2011) **38**, 1-11.

68 Guerrero, S. *et al.* Synthesis and in vivo evaluation of the biodistribution of a 18F-labeled conjugate gold-nanoparticle-peptide with potential biomedical application. *Bioconjugate chemistry* (2012) **23**, 399-408.

69 Säterborg, N. E. The distribution of 198Au injected intravenously as a colloid and in solution. *Acta Radiologica: Therapy, Physics, Biology* (1973) **12**, 509-528.

70 Balogh, L. *et al.* Significant effect of size on the in vivo biodistribution of gold composite nanodevices in mouse tumor models. *Nanomedicine* (2007) **3**, 281-296.

71 Hillyer, J. F. & Albrecht, R. M. Gastrointestinal persorption and tissue distribution of differently sized colloidal gold nanoparticles. *J Pharm Sci* (2001) **90**, 1927-1936.

72 Huang, K. *et al.* Size-dependent localization and penetration of ultrasmall gold nanoparticles in cancer cells, multicellular spheroids, and tumors in vivo. *ACS Nano* (2012) **6**, 4483-4493.

73 Cedervall, T. *et al.* Understanding the nanoparticle–protein corona using methods to quantify exchange rates and affinities of proteins for nanoparticles. *Proceedings of the National Academy of Sciences of the United States* (2007) **104**, 2050–2055.

74 Casals, E. & Puntes, V. F. Inorganic nanoparticle biomolecular corona: formation, evolution and biological impact. *Nanomedicine (Lond)* (2012) **7**, 1917-1930.

75 König, G. Proteins (blue-green) enclose a nanoparticle (green) that can bind to the cell membrane, e.g. to receptors (blue), like the free protein. (Graphics by: CFN). http://www.kit.edu/english/55_450.php (Stand: 29.01.2013).

76 Lipka, J. *et al.* Biodistribution of PEG-modified gold nanoparticles following intratracheal instillation and intravenous injection. *Biomaterials* (2010) **31**, 6574-6581.

77 Niidome, T. *et al.* PEG-modified gold nanorods with a stealth character for in vivo applications. *Journal of controlled release : official journal of the Controlled Release Society* (2006) **114**, 343-347.

78 Jokerst, J. V., Lobovkina, T., Zare, R. N. & Gambhir, S. S. Nanoparticle PEGylation for imaging and therapy. *Nanomedicine (Lond)* (2011) **6**, 715-728.

79 Simpson, C. A., Salleng, K. J., Cliffel, D. E. & Feldheim, D. L. In vivo toxicity, biodistribution, and clearance of glutathione-coated gold nanoparticles. *Nanomedicine* (2013) **9**, 257-263.

80 Hirn, S. *et al.* Particle size-dependent and surface charge-dependent biodistribution of gold nanoparticles after intravenous administration. *Eur J Pharm Biopharm* (2011) **77**, 407-416.

81 Schleh, C. *et al.* Size and surface charge of gold nanoparticles determine absorption across intestinal barriers and accumulation in secondary target organs after oral administration. *Nanotoxicology* (2012) **6**, 36-46.

6 Publikationen

6.1 Particle size-dependent and surface charge-dependent biodistribution of gold nanoparticles after intravenous injection

European Journal of Pharmaceutics and Biopharmaceutics 77 (2011) 407–416

Contents lists available at ScienceDirect

European Journal of Pharmaceutics and Biopharmaceutics

journal homepage: www.elsevier.com/locate/ejpb

Research paper

Particle size-dependent and surface charge-dependent biodistribution of gold nanoparticles after intravenous administration

Stephanie Hirn [a], Manuela Semmler-Behnke [a], Carsten Schleh [a], Alexander Wenk [a], Jens Lipka [a], Martin Schäffler [a], Shinji Takenaka [a], Winfried Möller [a], Günter Schmid [b], Ulrich Simon [c], Wolfgang G. Kreyling [a,*]

[a] Helmholtz Center Munich – German Research Center for Environmental Health, Neuherberg – Munich, Germany
[b] Institute of Inorganic Chemistry, University Duisburg-Essen, Essen, Germany
[c] Institute of Inorganic Chemistry, RWTH Aachen University, Aachen, Germany

ARTICLE INFO

Article history:
Available online 31 December 2010

Keywords:
Gold nanoparticles
Intravenous injection
Female Wistar-Kyoto rat
In vivo biodistribution
Nanoparticle size and surface charge
Hepato-biliary and renal clearance

ABSTRACT

Gold nanoparticles (GNP) provide many opportunities in imaging, diagnostics, and therapies of nanomedicine. Hence, their biokinetics in the body are prerequisites for specific tailoring of nanomedicinal applications and for a comprehensive risk assessment.

We administered ^{198}Au-radio-labelled monodisperse, negatively charged GNP of five different sizes (1.4, 5, 18, 80, and 200 nm) and 2.8 nm GNP with opposite surface charges by intravenous injection into rats. After 24 h, the biodistribution of the GNP was quantitatively measured by gamma-spectrometry.

The size and surface charge of GNP strongly determine the biodistribution. Most GNP accumulated in the liver increased from 50% of 1.4 nm GNP to >99% of 200 nm GNP. In contrast, there was little size-dependent accumulation of 18–200 nm GNP in most other organs. However, for GNP between 1.4 nm and 5 nm, the accumulation increased sharply with decreasing size; i.e. a linear increase with the volumetric specific surface area. The differently charged 2.8 nm GNP led to significantly different accumulations in several organs.

We conclude that the alterations of accumulation in the various organs and tissues, depending on GNP size and surface charge, are mediated by dynamic protein binding and exchange. A better understanding of these mechanisms will improve drug delivery and dose estimates used in risk assessment.

1. Introduction

The use of engineered nanoparticles (NP) offers a huge potential in the field of nanomedicine and nanotechnologies in the future. Especially, gold nanoparticles (GNP) provide several opportunities in imaging, diagnostics, and therapies [1–3]. Their widespread use, their relatively simple generation and surface modification, and their special physico-chemical characteristics make GNP attractive candidates for the detection of cancerous cells as well as in tumor targeting [4–6]. There are, therefore, numerous studies concerning the properties of GNP as drug carriers [1,2,7]. Moreover, different administration routes such as inhalation, ingestion, or intravenous (i.v.) injection are possible. The advantage of this latter administration route is the direct access to the blood circulation and thereby a rapid distribution throughout the entire body.

Nevertheless, the investigation of cytotoxic effects is crucial. Based upon in vivo studies, no toxic effects of 12.5 nm GNP are found in the liver, lungs, kidneys, spleen or brain [8,9]. Also, toxicity assessments of GNP of different sizes (3 nm, 10 nm, 50 nm, and 100 nm) in zebrafish embryos showed only minimal sub-lethal toxic effects [10]. A size-dependent toxic impact of GNP was investigated in vitro, which occurred for 1.4 nm GNP, but not for 15 nm, or 0.8 nm GNP [11]. The findings of the extraordinary cytotoxicity of the 1.4 nm GNP were explained by the perfect fitting of these GNP in the major grooves of the DNA causing its immobility [9]. In addition, the cellular uptake of GNP varies with size and shape causing effects, which need to be considered in determining the design of the nanomaterial [12].

Moreover, an important focus in order to achieve safe and well-characterized tools for nanomedicine is the in vivo biodistribution of candidate NP as this will allow for determining the GNP dose to secondary organs, which may eventually cause adverse health effects. Interestingly, commercially available 1.9 nm GNP used as X-ray contrast agents, were surface modified "with a highly water soluble organic shell" (but not explicitly disclosed) such that they were excreted almost quantitatively via urine [13] making them

* Corresponding author. Comprehensive Pneumology Center, Helmholtz Zentrum München, Institute of Lung Biology and Disease, Focus Network Nanoparticles and Health, Ingolstädter Landstraße 1, 85764 Neuherberg, Germany. Tel.: +49 (0)89 3187 2309; fax: +49 (0)89 3187 3397.
E-mail address: kreyling@helmholtz-muenchen.de (W.G. Kreyling).

0939-6411/$ - see front matter © 2011 Elsevier B.V. All rights reserved.
doi:10.1016/j.ejpb.2010.12.029

ideal diagnostic tools without long-lasting residence time in the body. Similarly, 4 h after i.v. injection the renal clearance of ^{99m}Tc-labeled, cysteine-surface-modified quantum dots (QD) with hydrodynamic diameters of <5.5 nm was shown by a strong QD increase of up to 80% in the urine. While for QD, with a hydrodynamic diameter of 8.65 nm, the uptake in the liver reached 26.5% of injected dose (ID) and it was 6.3% ID [14] for the spleen.

Also, surface charge affects the biodistribution of GNP so that positively charged particles accumulate more in the kidneys while negative and non-charged particles showed a higher accumulation in the liver [15].

Once retained in the liver, the hepato-biliary pathway allows for clearance through the biliary duct into the duodenum. The daily excretion of 20 nm low-density lipoprotein-GNP through the biliary duct was almost 5% from 4 to 12 days after i.v. administration [16]. For 50–100 nm sized mesoporous silica nanoparticles, a rapid hepato-biliary transport (within <30 min was shown for highly charged particles) while less charged NP remained in the liver [17] for up to over 90 days.

The aim of the present study was to evaluate the biodistribution of monodisperse, spherical GNP of different sizes with well-defined surface ligands of different surface charges. Therefore, a large size range of five different sizes (1.4 nm, 5 nm, 18 nm, 80 nm and 200 nm) of mono-sulfonated triphenylphosphine (TPPMS) stabilized GNP, as well as opposite surface charge, with either positive cysteamine (CA) charge or negative thioglycolic acid (TGA) charge of equal size (2.8 nm) were intravenously injected into healthy adult female rats. All GNP were radioactively labeled with ^{198}Au allowing for a 100% balanced quantitative determination of the GNP biodistribution after 24 h. Our study aims to serve as a proof-of-principle for the validity of a systematic investigation of size and surface charge of GNP. Therefore, in this study, we present the 24 h body distribution after i.v. injection of GNP. These initial studies need to be followed up by a complete kinetic study with more time points which are, however, currently under scrutiny.

2. Methods

2.1. Animals

Healthy, female Wistar-Kyoto rats (WKY/Kyo@Rj rats, Janvier, Le Genest Saint Isle, France), 8–10 weeks old (approximately 250 g body weight) were housed in pairs in humidity- and temperature-controlled ventilated cages on a 12-h day/night cycle.

A rodent diet and water were provided ad libitum. All experiments were conducted under German Federal guidelines for the use and care of laboratory animals and were approved by the Regierung von Oberbayern (Government of District of Upper Bavaria, Approval No. 211-2531-94/04) and by the Institutional Animal Care and Use Committee of the Helmholtz Center Munich.

2.2. Nanoparticle preparation and characterization

Mono-sulfonated triphenylphosphine (TPPMS) stabilized GNP (Table 1) (1.4 nm and 18 nm) were synthesized following previously published procedures [11]. Citrate stabilized, spherical GNP (5 nm, 80 nm, 200 nm) were purchased from Plano (Wetzlar, Germany). Ligand exchange (citrate to TPPMS) was accomplished as previously described [11].

The fabrication of the 2.8 nm GNP followed the same procedure as described in [11] by performing ligand exchange of initially 1.4 nm GNP stabilized with triphenylphosphine (TPP). Via phase transfer from a dichloromethane phase to an aqueous phase TPP is replaced by thioglycolic acid (TGA) for carboxylated, negatively charged GNP and by cysteamine (CA) for aminated, positively charged particles, respectively. The driving force for this exchange reaction is the higher binding affinity of thiol groups to gold compared to phosphine groups accompanied with the change in polarity, since the GNP pass from the dichloromethane phase into the aqueous phase, when TPP is replaced by TGA or CA, respectively. Hence, the solubility/dispersion of the GNP in water gives immediate evidence that the ligand exchange was successful.

As has already been observed by others, the replacement of TPP by thiol ligands is associated with a growth of the gold core [18,19]. This also holds for our ligand exchange procedure, where the introduction of thiol ligands TGA and CA resulted in an increase in the mean core particle size, which was determined by TEM analyses to be 2.8 ± 0.4 nm for both ligands.

All GNP were activated by neutron irradiation (^{197}Au (n, γ) ^{198}Au). For this, the GNP were activated at a neutron flux of 10^{14} cm^{-2} s^{-1} at the research reactor of the Helmholtz Center Berlin (formerly Hahn-Meitner Institute, Berlin), Germany. Gold amounts and irradiation times were adjusted to provide sufficient ^{198}Au radioactivity for the subsequent in vivo studies. Specific ^{198}Au radioactivity and the isotope ratio of ^{198}Au to stable ^{197}Au are given in Table 1. Note that this ratio is extremely low so that statistically, only one ^{198}Au isotope can be found in all GNP from 1.4 nm to 18 nm and most of the GNP do not contain any ^{198}Au atom at all; but in the 80 nm and 200 nm GNP an average number of 20 and 300 ^{198}Au atoms, respectively, are contained in the NP matrix, Table 1.

After the neutron irradiation immediately prior to rat application, the 1.4 nm and the 2.8 nm ^{198}Au-NP solution was filtered through a 10 cm column of Celite to remove agglomerates; losses determined by ^{198}Au radioactivity accounted for about 10%. All other ^{198}Au-NP suspensions from 5 nm to 200 nm were visually controlled for precipitates and their correct pink translucent colour of the colloidal suspension immediately prior to the application in rats; no changes were found when compared to the suspension prior to irradiation.

The hydrodynamic diameters (HD) and the polydispersity index (PdI) of the all NP from 5 nm to 200 nm were measured in duplicate by photon correlation spectroscopy (PCS; Malvern HPPS5001 or Nano Zetasizer ZS, Herrenberg, Germany). The HD were slightly increased compared to the core GNP diameters according to the surface modifications, and a minute fraction of agglomerates was sometimes observed (however, when NP volume and not the intensity was plotted, the fraction of agglomerates disappeared; data not shown). The aqueous GNP solutions of 1.4–18 nm NP suspension remained stable during at least two weeks without any detectable precipitation or change of color. Due to gravitational sedimentation, 80 nm and 200 nm GNP settled during the two weeks but could, by vortexing, be dispersed into the same pink suspension as before.

Zeta-potential measurements were made in duplicate using appropriate working dilutions in a Zetapalssystem (Brookhaven Instruments Corporation, Holtsville and later using Nano Zetasizer, Malvern, Herrenberg). The NP suspensions were diluted with purified water to adjust the concentration level (ratio 1:1). Measurements were made in duplicates (10 cycles each run).

2.3. Nanoparticle administration and animal maintenance in metabolic cages

Nanoparticle suspensions were administered to the animals via i.v. injection. The rats were anesthetized by inhalation of 5% isoflurane until muscular tonus relaxed. The rats were kept under isoflurane anesthesia and a flexible i.v. catheter (24 G, ¾ in) was placed into the tail vein. Subsequently, 120 µl of the suspension was slowly injected using a 1-ml insulin syringe (dead space of syringe connector and catheter was determined to vary between 50 and

Table 1
Physico-chemical parameters and dose metrics of administered ^{198}Au-NP and their radioactive labels; additionally does metrics of ^{198}Au-NP mass, surface area, number, and doses delivered to each rat by i.v. injection.

Gold NP, core diameter (nm)	1.4	5	18	80	200	2.8	2.8
Surface modification, ligand	TPPMS	TPPMS	TPPMS	TPPMS	TPPMS	TGA (COO^-)	CA (NH_3^+)
Hydrodynamic diameter (nm)	2.9[a]	12.1[c]	21[c]	85[b]	205[b]	ND[d]	ND[d]
Polydispersity index (PdI)	ND	0.19	0.10	0.12	0.05	ND[d]	ND[d]
pH Value of suspension	5.6	5.8	6.4	5.4	5.5	ND	ND
Zeta-potential (mV)	−20.6 ± 0.5	−21.1 ± 1.4	−22.8 ± 3.1	−22.3 ± 1.6	−41.3 ± 4.5	Negative	Positive
Specific ^{198}Au radioactivity (GBq/g)	72	6.7	31	14.9	11.5	15.8	5.5
Isotope ratio of ^{198}Au to stable ^{197}Au	8.0×10^{-6}	7.4×10^{-7}	3.4×10^{-6}	1.7×1^{-6}	1.3×10^{-6}	1.7×10^{-6}	6.1×10^{-7}
Ratio of ^{198}Au per NP	6.6×10^{-4}	2.8×10^{-3}	0.60	26	307	1.2×10^{-3}	4.1×10^{-4}
Admin. ^{198}Au radioactivity (kBq) per rat	0.22 ± 0.05	0.21 ± 0.3	0.09 ± 0.05	0.28 ± 0.03	0.23 ± 0.02	0.025 ± 0.003	0.16 ± 0.02
Admin. mass of gold NP (μg) per rat	3.1 ± 0.6	43.7 ± 5.3	2.9 ± 1.5	18.5 ± 2.3	19.8 ± 1.7	1.6 ± 0.2	29.0 ± 3.4
Admin. number of gold NP per rat	$1.1 \pm 0.2 \times 10^{14}$	$3.5 \pm 0.4 \times 10^{13}$	$5.1 \pm 2.6 \times 10^{10}$	$3.6 \pm 0.5 \times 10^{9}$	$3.9 \pm 0.3 \times 10^{9}$	$7.3 \pm 0.9 \times 10^{12}$	$1.3 \pm 0.2 \times 10^{14}$
Admin. Surface Area (cm^2)	7.0 ± 1.4	27.6 ± 3.4	0.56 ± 0.27	0.73 ± 0.09	0.78 ± 0.07	1.4 ± 0.2	26.0 ± 3.0

TPPMS, Triphenylphosphine mono-sulfonate; TGA (COO^-), thioglycolic acid (mercaptoacetic acid); CA (NH_3^+), cysteamine (2-aminoethanethiol).
ND not determined.
[a] As determined earlier [47].
[b] DLS measurement using Malvern HPPS5001, Herrenberg, Germany; in addition, TEM and UV/vis analyses confirmed the core size of the gold NP [21].
[c] DLS measurement using Malvern Zetasizer Nano ZS, Herrenberg, Germany.
[d] Hydrodynamic diameter and PdI were not determined but the mean core size ± STD of both batches of GNP already surface modified with either the carboxyl or the amino groups used were determined to be 2.8 ± 0.4 nm.

70 μl) resulting in an effectively injected GNP suspension volume of 70–50 μl.

2.4. Retention and excretion

After the i.v. injection and recovery from anesthesia, each rat was kept isolated in metabolic cages for the next 24 h and the urine and feces were collected separately and quantitatively.

2.5. Sample preparation

Twenty-four hours after administration, the rats were anesthetized (5% isoflurane inhalation) and euthanized by exsanguination via the abdominal aorta. Approximately 70% of the total blood volume was withdrawn based on an estimation of the total blood volume of the body weight [20]. For radio-analysis, organs – each in toto – and tissues listed below, as well as total excretion and the entire remaining carcass, were collected as previously described [21].

- Organs: lungs, liver, spleen, kidneys, brain, heart, uterus, gastrointestinal tract (GIT): esophagus, stomach, small and large intestine;
- Tissues: the injected site of the tail was separated;
- Remainder: total remaining carcass (skin, skeleton, soft tissue) beyond the listed organs and tissues;
- Excretion: total urine and feces, collected separately
- Total exsanguinated blood

During dissection, no organs were cut and all fluids were cannulated where necessary in order to avoid cross-contaminations.

The hepato-biliary GNP clearance was calculated summing up the GNP percentages determined by the small intestine, colon and total fecal excretion; it describes the biliary pathway from the liver into the small intestine and subsequently into fecal excretion.

2.6. Radio-analysis

The ^{198}Au radioactivity of all samples was measured without any further physico-chemical preparation by γ-spectroscopy in either a lead-shielded 10 ml or a lead-shielded 1 l well type NaI(Tl) scintillation detector. The count rates were adjusted for physical decay and background radiation. Additionally, count rates were calibrated to a ^{198}Au reference source at a reference date in order to correlate ^{198}Au radioactivities to the numbers, surface areas, and masses of the GNP. Samples yielding net counts (i.e. background-corrected counts) in the photo-peak region-of-interest of the ^{198}Au gamma spectrum less than three standard deviations of the totally measured counts were defined to be below the detection limit. For a complete balance of the administered ^{198}Au radioactivity within each rat, ^{198}Au radioactivities of all samples were summed for each rat and used as a denominator for the calculation of the ^{198}Au percentage of each sample.

2.7. Blood correction adjustment

Blood contents of organs and the remaining body were calculated according to the findings of Oeff et al. [20]. The NP content of the remaining blood volume of each sample was estimated and subtracted from the measured ^{198}Au radioactivity to obtain the absolute ^{198}Au activity of the tissue or organ. In the case of the carcass, the difference between the total blood volume of the animal (6.7% of the body weight [20]), the sum of all organ blood contents, and the collected blood sample was calculated to be the blood volume of the carcass.

2.8. Calculations and statistical analysis

All calculated values are given as a percentage of the relevant integral radioactivity of all samples in each animal with the standard deviation (SD).

All calculated significances are based on a one-way analysis of variance (ANOVA) followed by a post hoc Tukey test. In the case of an individual two group comparison, the unpaired t-test was used. The criterion for statistical significance was $p \leqslant 0.05$ if not otherwise stated. Outliers were identified by the Grubbs test and excluded.

3. Results

3.1. Particle characterization and administration

Physico-chemical parameters of all GNP are given in Table 1, indicating that the GNP were single and showing a narrow size distribution prior to in vivo injection; in addition, the mean

administered GNP mass, surface, and number doses per rat are listed in Table 1. Note that in the following, all GNP percentages of the administered GNP dose provided for organs and tissues represent exclusive GNP retention in the tissue without GNP of the blood volume in these organs and tissues – see Section 2.

3.2. Effect of TPPMS surface modified GNP size from 1.4 nm to 200 nm

Our studies showed a strong size dependency of the distribution and accumulation of GNP in all organs, tissues and excretions. GNP percentages per organ or tissue are given in Figs. 1A–J and 2A; GNP percentages of the ID per gram of organ or tissue are given in Table 2.

3.2.1. GNP retention in blood

Surprisingly, we found small but detectable percentages >0.1% of the administered GNP of all sizes in the blood, which were still circulating 24 h after administration, Fig. 1H. These percentages had a minimum at 5–18 nm and increased slightly to 200 nm. However, they increased even more sharply from 5 nm to 2.8 nm and 1.4 nm up to about 8%. This increasing percentage with decreasing GNP in the size ranged between 1.4 nm and 5 nm was proportional to the volumetric specific surface area (VSSA) [22] which corresponds to the inverse diameter 1/d of the GNP.

By distinguishing GNP retention in serum versus blood cells by means of centrifugation there was a 10-fold higher retention of 18 nm GNP in the cell fraction compared to the serum, indicating their binding, in part, to blood cells (since 18 nm GNP did not settle in an aqueous suspension under the same centrifugation condition). The same was also found for the 80 nm and 200 nm GNP. However, while 18 nm GNP did not settle in an aqueous suspension, detectable fractions of 80 nm and 200 nm GNP were spun down under the same centrifugation conditions indicating that the GNP may also have settled as free GNP. Fractions of 5 nm GNP were equally found in the serum and blood cells. The 1.4 nm GNP percentage in the serum was as high as 75% compared to 25% in blood cells.

3.2.2. GNP accumulation in the liver

After the i.v. injection, most GNP were rapidly eliminated from circulation and accumulated predominantly in the liver, Fig. 2A. However, while GNP accumulation was in the range from 91.9% to 96.9% for 5, 18, 80 and 200 nm GNP, the distribution of 1.4 nm and carboxylated 2.8 nm GNP showed significantly lower percentages of 51.3% and 81.6%, respectively. Hence, for 5, 18, 80 and 200 nm GNP accumulation in any other organ or tissue was only a few percent and even lower than 4% for 200 nm GNP, Fig. 1A–I. In contrast, almost 50% of the 1.4 nm GNP escaped being trapped in the liver and thus accumulated in the other organs and tissues as well as excretion. Interestingly, the negatively charged 2.8 nm GNP with a carboxyl surface coating fits very well into this size dependency pattern with 81.6 in the liver and hence almost 20% in the other organs and tissues as well as excretion, (Figs. 1A–I and 2A). When plotting liver accumulation AC_{liv} between 1.4 nm and 5 nm over the volume specific surface area (VSSA), it declined

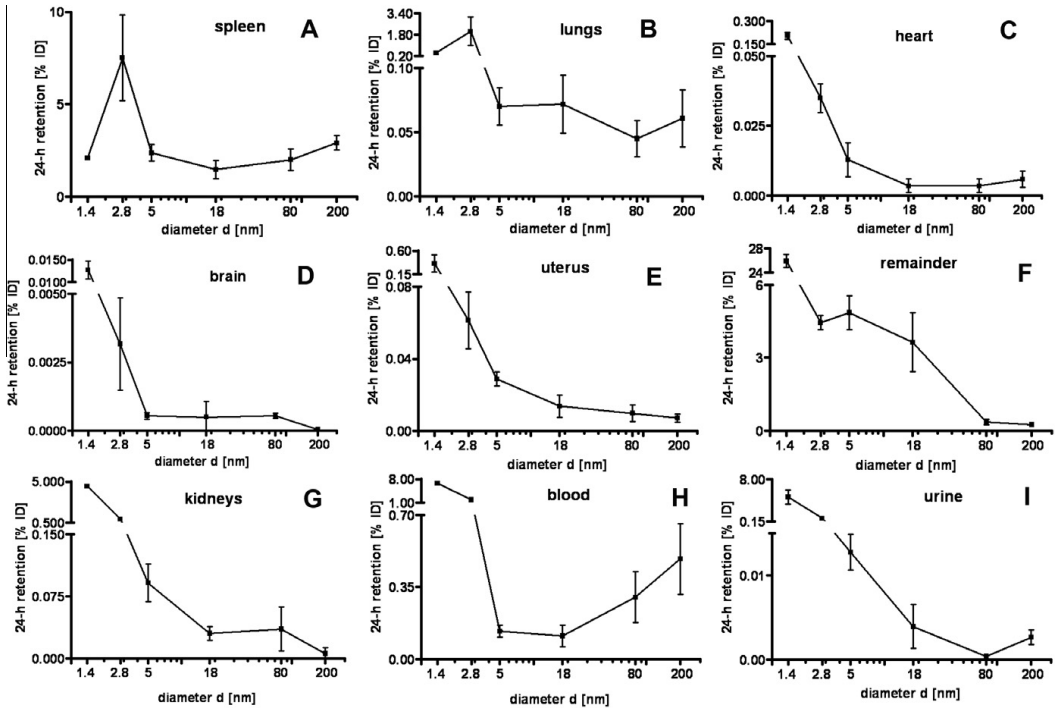

Fig. 1. Twenty-four hours retention/accumulation of intravenously injected, negatively charged, spherical GNP (1.4 nm, 5 nm, 18 nm, 80 nm, 200 mm coated with TPPMS; 2.8 nm carboxyl-coated); GNP percentages of initial dose are given for whole organs, the entire remaining carcass and total blood and urine; in each panel the respective organ, tissue or body fluid is indicated. Data are mean ± SD, $n = 4$ rats. Note log scale of x-axis.

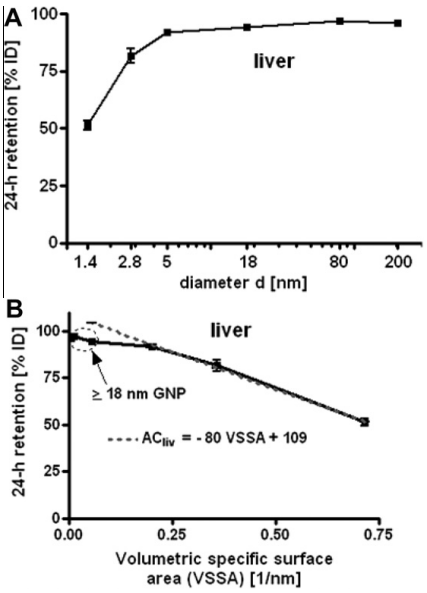

Fig. 2. Twenty-four hours liver accumulation of intravenously injected, negatively charged, spherical GNP (1.4 nm, 5 nm, 18 nm, 80 nm, 200 mm coated with TPPMS; 2.8 nm carboxyl-coated); GNP percentages of initial dose in whole liver. Panel A: Percentages plotted over GNP diameter in log scale. Panel B: Percentages plotted over the volumetric specific surface area (VSSA 1/d) of GNP. Data are mean ± SD, $n = 4$ rats. Note log scale of x-axis. Significant changes of accumulation of given GNP sizes versus those of all other GNP sizes are indicated as determined by the ANOVA test. ($^{*}p < 0.05$; $^{*}p < 0.01$; $^{a}p < 0.001$).

linearly with increasing VSSA (in 1/nm) of the GNP. This can be described with a linear equation:

$$AC_{liv} = -80 * VSSA + 109 \quad (R^2 = 0.99)$$

i.e. with increasing specific surface area fewer GNP are trapped in the liver, Fig. 2B.

For morphologic GNP identification in the liver we localized 18 nm GNP using transmission electron microscopy (TEM) (Fig. 3). These GNP were predominantly found in Kupffer cells, (panel A) but also, to a smaller extent, in endothelial cells (panel B) and in hepatocytes (panel C). In the endothelial cells and hepatocytes, the 18 nm GNP appeared mostly isolated while in Kupffer cells we found both small and large agglomerates of GNP.

3.2.3. GNP accumulation in spleen

The spleen, which exhibits macrophages in its vasculature like the liver, does not show a GNP size-dependent pattern, but the accumulated GNP percentages of around 2% were quite constant for all TPPMS-coated GNP ranging from 1.4 nm to 200 nm, Fig. 1A. However, the carboxyl-coated 2.8 nm GNP showed a significantly higher accumulation of 8.6% compared to all TPPMS-coated GNP. A significantly higher accumulation of 11.4% than those of all TPPMS-coated GNP was observed for the positively charged amino-coated 2.8 nm GNP, see Fig. 5A.

3.2.4. GNP accumulation in other organs and tissues

Regarding GNP size dependency, the liver is the only organ which showed increased accumulation with increasing GNP size. In contrast, most of the other organs, tissues, and blood showed quite a low and similar size-independent accumulation of GNP

Table 2
GNP concentrations per gram of organ, tissue or blood: 24 h retention/accumulation of intravenously injected GNP (1.4 nm, 5 nm, 18 nm, 80 nm, 200 mm coated with TPPMS; 2.8 nm carboxyl- and amino-coated); GNP concentrations are given as percentages of initial dose. Data are mean ± SD, $n = 4$ rats.

^{198}Au-GNP	1.4 nm	5 nm	18 nm	80 nm	200 nm	2.8 nm COO^-	2.8 nm NH_3^+
Liver	$5.1 \times 10^{0} \pm 4.8 \times 10^{-1}$	$1.0 \times 10^{+1} \pm 2.2 \times 10^{-1}$	$1.0 \times 10^{+1} \pm 1.1 \times 10^{0}$	$1.1 \times 10^{+1} \pm 1.3 \times 10^{0}$	$1.2 \times 10^{+1} \pm 1.3 \times 10^{0}$	$9.2 \times 10^{0} \pm 2.7 \times 10^{-1}$	$7.9 \times 10^{0} \pm 4.8 \times 10^{-1}$
Spleen	$2.3 \times 10^{0} \pm 2.4 \times 10^{-1}$	$2.7 \times 10^{0} \pm 1.2 \times 10^{0}$	$1.6 \times 10^{0} \pm 3.8 \times 10^{-1}$	$1.9 \times 10^{0} \pm 5.2 \times 10^{-1}$	$3.6 \times 10^{0} \pm 5.6 \times 10^{-1}$	$8.9 \times 10^{0} \pm 1.9 \times 10^{0}$	$1.3 \times 10^{1} \pm 1.4 \times 10^{0}$
Lungs	$2.0 \times 10^{-1} \pm 1.4 \times 10^{-1}$	$3.5 \times 10^{-2} \pm 5.1 \times 10^{-3}$	$3.8 \times 10^{-2} \pm 1.3 \times 10^{-2}$	$2.7 \times 10^{-2} \pm 1.1 \times 10^{-2}$	$3.7 \times 10^{-2} \pm 1.4 \times 10^{-2}$	$1.2 \times 10^{0} \pm 3.4 \times 10^{-1}$	$1.2 \times 10^{0} \pm 9.2 \times 10^{-2}$
Kidneys	$1.9 \times 10^{0} \pm 2.8 \times 10^{-1}$	$3.7 \times 10^{-2} \pm 1.0 \times 10^{-2}$	$1.3 \times 10^{-2} \pm 4.5 \times 10^{-3}$	$1.6 \times 10^{-2} \pm 1.3 \times 10^{-2}$	$2.5 \times 10^{-3} \pm 3.2 \times 10^{-3}$	$4.0 \times 10^{-1} \pm 2.8 \times 10^{-2}$	$4.8 \times 10^{-1} \pm 2.9 \times 10^{-2}$
Heart	$1.8 \times 10^{-1} \pm 5.4 \times 10^{-3}$	$6.9 \times 10^{-3} \pm 2.3 \times 10^{-3}$	$9.4 \times 10^{-3} \pm 3.5 \times 10^{-3}$	$3.4 \times 10^{-3} \pm 2.0 \times 10^{-3}$	$5.6 \times 10^{-3} \pm 2.2 \times 10^{-3}$	$3.9 \times 10^{-2} \pm 1.6 \times 10^{-3}$	$5.2 \times 10^{-2} \pm 1.6 \times 10^{-3}$
Brain	$6.4 \times 10^{-3} \pm 1.2 \times 10^{-3}$	$6.0 \times 10^{-5} \pm 4.3 \times 10^{-5}$	$3.1 \times 10^{-5} \pm 3.7 \times 10^{-5}$	$2.9 \times 10^{-4} \pm 6.8 \times 10^{-5}$	$2.1 \times 10^{-5} \pm 2.3 \times 10^{-5}$	$1.8 \times 10^{-3} \pm 4.0 \times 10^{-4}$	$2.8 \times 10^{-3} \pm 2.2 \times 10^{-4}$
Uterus	$1.8 \times 10^{-1} \pm 5.1 \times 10^{-2}$	$7.9 \times 10^{-3} \pm 1.2 \times 10^{-3}$	$3.7 \times 10^{-3} \pm 1.8 \times 10^{-3}$	$1.5 \times 10^{-3} \pm 7.5 \times 10^{-4}$	$1.2 \times 10^{-3} \pm 3.8 \times 10^{-4}$	$2.6 \times 10^{-2} \pm 2.8 \times 10^{-3}$	$3.2 \times 10^{-2} \pm 5.1 \times 10^{-3}$
Remainder	$3.5 \times 10^{-1} \pm 2.1 \times 10^{-2}$	$7.7 \times 10^{-3} \pm 1.6 \times 10^{-3}$	$5.9 \times 10^{-3} \pm 3.0 \times 10^{-3}$	$1.6 \times 10^{-3} \pm 6.6 \times 10^{-3}$	$2.6 \times 10^{-2} \pm 9.4 \times 10^{-3}$	$2.2 \times 10^{-2} \pm 1.1 \times 10^{-3}$	$4.4 \times 10^{-2} \pm 2.6 \times 10^{-3}$
Blood	$1.1 \times 10^{-1} \pm 6.0 \times 10^{-3}$	$2.4 \times 10^{-2} \pm 3.6 \times 10^{-3}$	$1.6 \times 10^{-2} \pm 6.6 \times 10^{-3}$	$1.6 \times 10^{-3} \pm 5.0 \times 10^{-4}$	$8.6 \times 10^{-4} \pm 6.0 \times 10^{-4}$	$1.1 \times 10^{-1} \pm 3.0 \times 10^{-3}$	$9.5 \times 10^{-2} \pm 5.2 \times 10^{-3}$

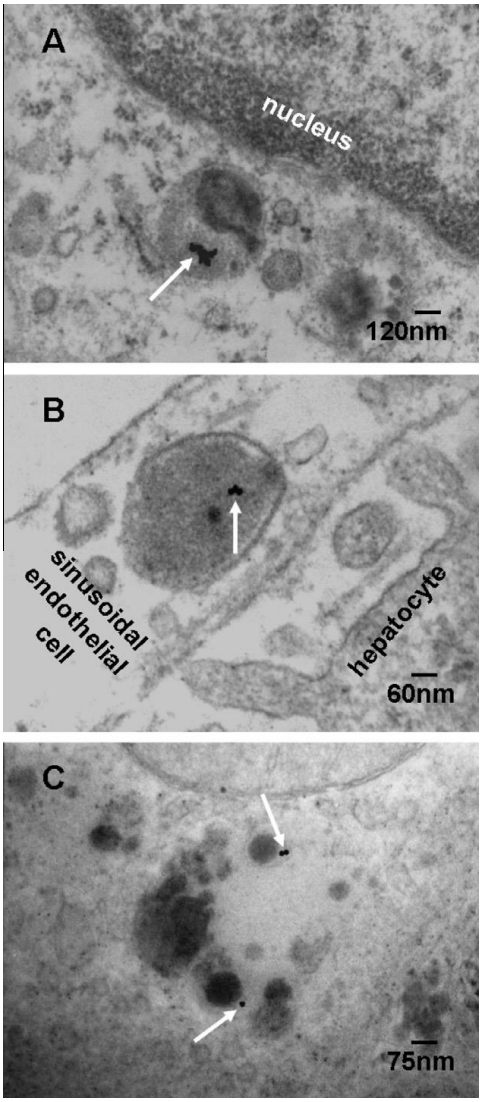

Fig. 3. Transmission electron micrographs of TPPMS-coated 18 nm GNP in a Kupffer cell (GNP agglomerate) (panel A), an endothelial cell (panel B) and a hepatocyte (panel C); arrows point towards GNP.

ranging from 18 nm to 200 nm size: the kidneys, heart, brain, uterus, remainder (Fig. 1C–G). Yet, this size-independent accumulation of 18 nm, 80 nm, and 200 nm GNP varies considerably among these organs and tissues. In contrast, from 5 nm to 2.8 nm and 1.4 nm GNP the accumulation rose sharply with decreasing GNP size (Fig. 1C–G). Interestingly, the accumulated percentages of the small GNP were proportional to the volumetric specific surface area (VSSA), which is inversely related to the diameter $1/d$. Slopes of the linear equation were determined by data fitting for each organ, remaining carcass, and blood, (see Table 3).

This described pattern was found for all TPPMS-coated GNP accumulated in the lungs, Fig. 1B; i.e. a constant percentage from

Table 3
Slope m of organ accumulation AC over VSSA for GNP of 1.4 nm to 2.8 nm to 5 nm diameter; slopes were determined by data fitting obtained from each organ, or remaining carcass or blood by the linear equation $AC_{org} = m * VSSA + b$; R^2 is coefficient of determination.

Organ, tissue or body fluid	Slope m, (%/d^{-1})	R^2
Kidneys	8.8	0.98
Heart	0.39	0.96
Brain	0.024	0.99
Uterus	0.67	0.96
Remainder	44	0.90
Blood	13	0.99
Urine	9.5	0.97

18 nm to 200 nm of about 0.06% and a significant increase from 0.07% for 5 nm GNP to 0.43% of 1.4 nm was observed. However, the carboxyl-coated 2.8 nm GNP showed a much higher accumulation than all TPPMS-coated GNP. This pattern corresponded to the pattern in spleen, Fig. 1A.

Interestingly, the remaining carcass, consisting of the skeleton and soft tissue (muscle, fat, skin), showed significantly higher percentages of the ID compared to all organs except the liver, Fig. 1F. These high percentages relate to the high mass of the remaining carcass since the GNP percentages per gram of carcass are quite low, Table 2. GNP retention in the carcass followed the same size dependency pattern as the blood and other organs, Fig. 1F.

Additionally, the collected urine during the 24 h after GNP application also showed a two-phase pattern with size-independent percentages of about 0.004% for 18–200 nm GNP, and a size-dependent VSSA proportional increase with the significantly highest percentage of 4.7% for the 1.4 nm GNP.

3.2.5. Hepato-biliary GNP clearance

The hepato-biliary GNP clearance describes the biliary pathways from the liver into the small intestine and subsequently into fecal excretion. Hepato-biliary clearance of the TPPMS-coated GNP showed an inverse linear relationship to the GNP diameter over the size range of 5–200 nm. The linear equation is given in Fig. 4. The clearance of the carboxylated 2.8 nm GNP also fit into this equation. Only the smallest GNP of 1.4 nm did not follow this size relationship and were cleared with the highest percentage of 4.6 ± 0.4%, which was significantly higher than for all other GNP.

3.2.6. GNP dose dependency

In order to check for GNP dose-dependent biodistribution we performed an additional study using a 20-fold mass dose of

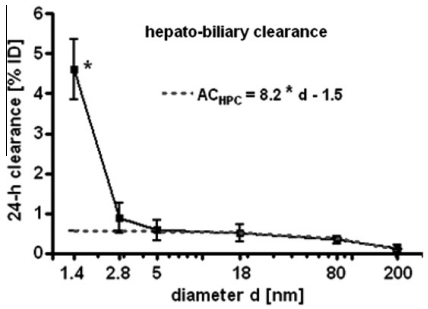

Fig. 4. Hepato-biliary clearance of GNP from the liver to the small intestine and fecal excretion; percentages of initial GNP dose of intravenously injected, negatively charged GNP (1.4 nm, 5 nm, 18 nm, 80 nm, 200 mm coated with TPPMS; 2.8 nm carboxyl-coated). Data are mean ± SD, $n = 4$ rats. Linear equation is fitted for data from 2.8 nm to 200 nm GNP. Note the log scale of x-axis bends the linear line. Significant change of accumulation of 1.4 nm GNP versus those of all other GNP sizes is indicated as determined by the ANOVA test. ($^*p < 0.05$).

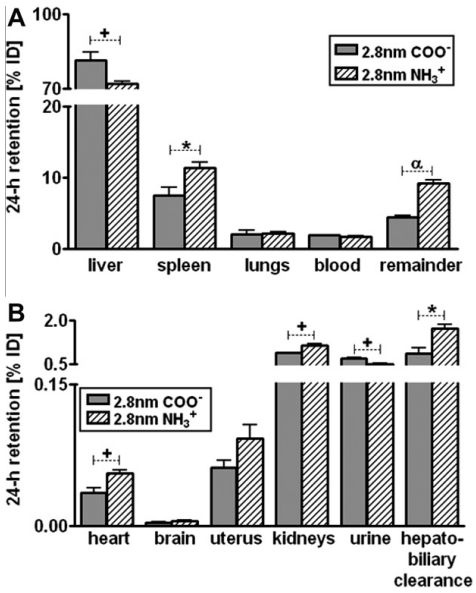

Fig. 5. Percentages of 24 h retention/accumulation of intravenously injected, 2.8 nm GNP (coated either with thioglycolic acid or with cysteamine); panel A: data obtained from liver, spleen, lungs, blood, remaining carcass; panel B: data obtained from heart, brain, uterus, kidneys urine and hepato-biliary clearance are given. Data are mean ± SD, $n = 4$ rats. Significant changes of accumulation of given GNP sizes versus those of the other GNP sizes are indicated as determined by the ANOVA test. ($^{*}p < 0.05$; $^{+}p < 0.01$; $^{\alpha}p < 0.001$).

1.4 nm GNP. The entire biodistribution 24 h later did not significantly differ for each organ, tissue, and body fluid from the data reported here (data of the 20-fold mass dose are not shown).

3.3. Effect of Surface charge of 2.8 nm carboxylated versus aminated GNP

After 24 h, most of the applied GNP, either negatively or positively charged, were found in the liver. These were significantly higher for negative 2.8 nm GNP (81%) than for positive 2.8 nm GNP (72%) (Fig. 5A). In contrast, in the spleen the positively charged GNP showed a significantly higher accumulation of 11.4% than the negative GNP of 8.6%, Fig. 5A. Both are factors of 6 and 5, respectively, and higher than for the TPPMS-coated GNP, Fig. 1A. For the lungs, an increased accumulation of carboxyl- and amino-coated GNP by a factor of 10 was observed compared to the TPPMS-coated GNP.

For the heart, kidneys, and remaining carcass, the negative GNP accumulated significantly less than the positive GNP (Fig. 5B). But in the urine, a significantly higher amount of negative GNP (0.71%) than positive GNP (0.51%) was detected.

Significantly more positively than negatively charged GNP were cleared through the hepato-biliary pathway (Fig. 5B).

4. Discussion

4.1. Physiological GNP dose

This study aims to determine quantitative, but macroscopic NP distribution at a GNP dose of no acute toxicity to any of the organs and tissues of the rats. The usage of precisely determined doses for measuring the biodistribution of GNP is challenging. In fact, we observed variable GNP retentions in the syringe and cannula with which the GNP suspensions were injected intravenously into the tail vein. This attributed systematically to the dead space of the syringe and cannula of about 50–70 μl, but also to additional incidental wall losses, which we carefully determined by radio-analysis at each application and was used for the proper correction of GNP dose delivery to the rat. In our recent study, we intentionally aimed for low GNP doses and did not apply more than 0.17 mg/kg body weight. Whereas in other studies found in open literature, doses between 0.1 and 2700 mg/kg body weight were administered (see Table 1 in [18]), our low GNP dose assures that it is very unlikely to expect any acute toxic effects or responses of the GNP surrounding tissues. These low mass doses became possible, including their detection, in the various organs, tissues, and excreta over a dynamic range of five orders of magnitude by using a stable-confined, radioactive ^{198}Au label of the GNP. The independence of GNP dose at this low end was demonstrated by an additional 24 h biodistribution study using a 20-fold higher mass dose of 1.4 nm GNP; the entire biodistribution in each organ, tissue, and the blood did not significantly differ from the lower dose data reported here.

Furthermore, we radio-labelled the GNP by neutron activation only to the extent required to detect the GNP in the various samples. As a result, the delivered radio-dose was far below the level required to cause any acute radio-toxic effect – even on a nanoscopic level, with the small GNP from 1.4 nm to 18 nm consisting of maximally one radio-isotope per GNP and the 80 nm and 200 nm GNP consisting, on average, 20 and 300 radio-isotopes per GNP. Such low numbers of radio-atoms clearly excludes any radio-dose effect in the direct vicinity of these NP and, at the same time, also warrants no instabilities of the gold core lattice. Using ^{198}Au as a radio-isotope of the same chemical element as the GNP provides the same chemistry of both radio-isotope and core NP matrix, thereby, preventing leaching of the radio-isotope out of the insoluble matrix of the gold NP. Yet, the selection of such rigid experimental parameters has some implications on experimental outcomes. Admittedly, these are the morphologic localisations within the tissues, which are impossible to detect for neither the very small nor the very large GNP. In fact, the localization of 1.4 nm and 2.8 nm GNP in biological tissue matrix are currently impossible with any electron microscopy technology (high resolution TEM imaging of these small NP requires a very clean substrate surface). Additionally, the silver enhancement method does not work for such small gold NP below 3 nm either, because of the lack of silver binding [23]. On the other hand, for 80 nm and 200 nm GNP, the number of GNP and the required magnification of the micrographs requires complete screening of thousands of 2–5 μm × 2.5 μm grid fields for electron microscopic examination, making it virtually impossible to detect these GNP in organs and tissues which have accumulated from less than 1% of the administered dose. Here, we show 18 nm GNP in Kupffer cells, as well as endothelial cells, and hepatocytes. Particularly, the single 18 nm GNP found in hepatocytes and endothelial cells indicate little agglomeration in the blood Fig. 3A–C. Increasing agglomeration of GNP in Kupffer cells over retention time has recently been reported [24] and may indicate agglomeration within the Kupffer cell as a result of endosomal fusion.

4.2. Protein coating

Changes in protein coatings of GNP are likely to cause a different biokinetic behavior of these GNP. It is well known, and it was recently confirmed, that PEGylation of 5 nm GNP induced prolonged blood circulation times; so different bioaccumulations

occur for PEGylated versus phosphinated GNP [25]. There is growing evidence that numerous serum proteins bind to negatively and positively charged NP [26,27]; for example, binding patterns were reported for quantum dots, gold, silica, polystyrene-latex, and copolymeric NP [14,15,28–32]. Additionally, in a recent study (ACS Nano 2009), the biochemistry of the binding of several important serum proteins to gold nanoparticles between 5 and 100 nm was thoroughly investigated in a size-dependent manner. Thereby the hydrodynamic diameter can increase by as much as a factor of two [31]. It was shown that the phosphor binding site of TPPMS-coated GNP can be substituted or detached in biologic systems while a disulfide bridge remains stable [33]. In our experiment, we used phosphinated GNP and therefore hypothesize that TPPMS coating is rapidly being replaced by proteins. In the case of the carboxylated or aminated GNP-protein, binding may occur to the surface molecules and/or after replacement of them. In any case, the GNP-protein-conjugate grows considerably in its hydrodynamic size and the original charge may change, and even alternate, according to the protein pattern on the GNP surface.

4.3. Charge dependency of 2.8 nm sized GNP

The distribution of GNP with the same 2.8 nm size depends on their charge. The significantly lower accumulation of positively charged 2.8 nm GNP in the liver may explain the mostly significantly higher accumulation in the other organs and in the remainder than for the negatively charged GNP. Yet, the binding of different serum proteins as a result of the different GNP charges and surface molecules is another option for the different accumulation pattern (Fig. 5A and B), which requires further investigation.

It was shown that the surface charge influences the toxicity of GNP. While anionic GNP appear non-toxic the cationic GNP were found to be moderately toxic, which resulted from their interaction with the cell membrane [34]. Moreover, a microscopic evaluation demonstrated the uptake of neutral and negative GNP by red blood cells while the positively charged GNP were attached to the cell surface [35]. This could also have influenced the biodistribution of the differently charged GNP.

In this study, we also used GNP smaller than 10 nm, and to our knowledge, there are almost no other papers available on the biodistribution so far. There is one study, which focuses on the biodistribution of differently charged gold-dendrimers with a gold core diameter of 5 nm, but these NP are not comparable to our GNP since they exhibit a large dendrimeric shell and contain several 5 nm GNP in one dendrimer NP [15].

4.4. Dispersion in blood and kidney clearance towards urine

In physiology it is well described that molecular structures smaller than 50 kDa including NP below a hydrodynamic diameter of 5.5 nm are almost quantitatively cleared by the kidneys into the urine. This is shown for 1.9 nm Gold NP of undisclosed surface modification to be used as an X-ray contrast agent [13], and for quantum dots with zwitterionic surface coating [14,30]. Pan et al. [33] just recently suggested that the TPPMS coating is rapidly removed in an in vitro cell culture system so that the naked GNP surface is likely to bind proteins. If this change in surface modification occurs in the blood it is likely that the most abundant protein, albumin, will be the first to bind to these GNP which we have shown in our ongoing work (data not shown). Roecker and coworkers [36] showed that iron–platinum NP of 11 nm original size, with a negatively charged carboxyl surface coating, show a dense package of albumin binding to these NP which gain size of up to 17 nm. Since both the 1.4 nm GNP and the 2.8 nm GNP are smaller than a 3.5 nm sized albumin molecule, they may bind to one or a few albumin molecules according to their negative surface charge. Hence, the GNP may be hidden within the conjugate and its diameter is likely to increase >5.5 nm. At this size a reduced clearance of the kidneys is expected [30], which is consistent with our observation. The fact that our TPPMS-coated 1.4 nm GNP and 2.8 nm GNP of both positive and negative charges were not quantitatively cleared into the urine, but only percentages of up to 5%, clearly indicated that protein binding depends on the surface modification and GNP size. This is supported by the decreased renal clearance of those anionically or cationically coated QD, which bound serum proteins in vivo resulting in an increased QD-conjugate size [14]. The NP retention in the blood rose with an increase in the VSSA from 5 nm to 1.4 nm GNP; it ran in parallel with GNP retention in the kidneys, Fig. 1G and H; i.e. a higher GNP concentration in the blood led to a higher accumulation in the tissue of the kidneys. At the same time, the higher GNP concentration in the blood led to more clearance into the urine, Fig. 1I. As a result, the GNP percentage in the urine also ran in parallel with GNP percentage in the blood and kidneys and increased with VSSA, as indicated in Fig. 1G–I and the slope of the linear fit of the blood, kidneys, and urine in Table 3. All slopes were in a rather small range compared to the other organs and tissues. In comparison with another study, our findings of 5 nm GNP in urine were much lower [15].

The high fraction of 18 nm GNP associated with blood cells and, likewise, those of the 80 nm and 200 nm GNP are a plausible mechanism for explaining the prolonged 24 h circulation time in the blood. Further studies are needed in order to resolve these kinds of mechanisms including endocytosis by monocytes, as well as the incorporation in red blood cells as demonstrated recently [35,37]. In contrast, the high GNP percentages in blood serum of 1.4–5 nm GNP points towards different mechanisms such as conjugation with serum proteins [28,29], which are able to increase GNP hydrophilicity and dispersion in blood. In fact, Pan and co-workers [11] just recently reported rapid replacement of the TPPMS surface coating in an in vitro study allowing for avid binding of serum proteins to the highly negatively charged naked GNP surface area.

4.5. Accumulation in organs and tissues

Our findings of the highest percentages found in the liver for all sizes, and surface modifications agree with studies of other groups [18,38,39]. Especially, the early distribution study by Säterborg [40] shows comparable data; they also used radio-labelled GNP (25 nm) which are comparable to the 18 nm GNP used in our study. Their results are confirmation of our investigations as the highest accumulation is detected in the liver [40]. Another study investigated the biodistribution of GNP of different sizes [41]; however, it is difficult to compare it with our results because it is not clear where the injected GNP ended up. In fact, less than 1% of the given dose is detected for all examined organs together and it is unclear where the remaining 99% is retained. Also, their application of a non-physiological dose of 1 g/kg is much too high [41]. The size-dependent GNP accumulation appears to be biphasic with almost no size dependency of the 18–200 nm GNP, but with a linear relation to VSSA of the 1.4–5 nm GNP. This is surprising as the increasing GNP surface area per volume was expected to lead to an increased receptor mediated GNP binding and endocytosis by the Kupffer cells in the liver. In fact, the contrary is the case. It appears that GNP $\leqslant$ 5 nm are too small to be trapped by membrane receptors of Kupffer cells. Indeed, we expect that GNP uptake in the liver is known to start immediately after GNP injection (first path kinetics). At this early stage, only abundantly available proteins, such as albumin, may have bound to GNP, but the entire dynamics of in vivo protein binding and exchange on the surface of NP is not yet understood. Regarding increasing Brownian motion of GNP-protein-conjugates, which are decreasing in size appears to be plausible to counteract the binding process to membrane receptors of Kupffer cells. The diffusion

coefficiency of 5 nm GNP-protein-conjugates in water is 1.3×10^{-10} m^2 s^{-1}, respectively, while the diffusion coefficiency of a 50 nm conjugate is 1.3×10^{-11} m^2 s^{-1}. The equation for the diffusional displacement distance s is:

$s^2 = 2Dt$; with time t and the diffusion coefficient

$D \sim 1/d'$; with $d'$the diameter of the GNP – protein conjugate

According to this equation, the displacement distance is 0.51 and 0.16 μm, respectively, within 1 ms. The displacement distance of 510 nm/ms of a 5 nm NP is 100-fold of the NP diameter and appears to be sufficiently fast enough to hinder receptor binding of the Kupffer cells, while the rather low movement of 160 nm/ms of a 50 nm NP is just threefold of the NP diameter and may therefore less affect the receptor binding on the membrane.

However, in other organs, there is comparably little binding of 18 nm to 200 GNP and from 5 nm down to 1.4 nm binding and accumulation increases with increasing VSSA. This surface area proportional increase was expected in general, but the microscopic mechanisms leading to this increase are still not understood. However, an important determinant is the GNP concentration in blood, which also increased with increasing VSSA. The increasing presence of GNP is merely likely to increase the probability of retention. It is noteworthy that this biphasic size-dependent pattern applies to organs as diverse as the brain, uterus, heart and kidneys. The relatively high levels and the same pattern of size dependency in the remaining carcass underlines the role of blood circulation leading to a wide GNP distribution and accumulation throughout the entire body. Note that these considerations apply to the GNP retained in the organs and tissues, but not to the GNP amount suspended in the blood volume of each organ or tissue; the latter was estimated and subtracted from the measured GNP – see Section 2.

At later time points, abundant proteins are likely to be replaced by higher affinity proteins in the blood, which will change the accumulation patterns, not only in the liver, but also in other organs. The fact that we still find GNP in the blood 24 h after the i.v. injection sheds light on the dynamics of interactions of GNP with serum proteins and blood cells, as well as macrophages in the liver and spleen, and additionally with endothelial cells. The larger percentages of GNP with ⩾18 nm diameter found in blood cells may be one mechanism, among others, in preserving GNP retention in blood. Additionally, clearance processes within 24 h of the previously accumulated GNP in various organs and tissues cannot be excluded either.

Although GNP percentages in the brain are low, we consistently found accumulation of all GNP and this accumulation pattern fits into those of the blood, and several other organs being size independent of between 18 nm and 200 nm while accumulation increased with increasing VSSA from 5 nm to 1.4 nm. This emphasizes once more that the blood–brain barrier is not completely tight sealed for NP circulating in blood as we have previously shown for iridium NP and elemental carbon NP [42–44]. This may be a concern in the case of chronic exposure of biopersistent NP reaching blood circulation.

Interestingly enough, no size-dependent accumulation of about 2% of TPPMS-coated GNP of the initial GNP dose was observed in the spleen over the entire size range. This was unexpected since the spleen belongs to the reticulo-endothelial-system (RES) well known for its size-dependent particle accumulation; for instance, submicron-sized polystyrene particles ranging from 60 to 250 nm were accumulated in the spleen of rats from 0.3% to 6.5% of the ID [45]. However, the carboxylated, as well as the aminated 2.8 nm GNP, were accumulated by factors of 4 and 5, respectively, when compared to all TPPMS-coated GNP. The different behaviour between our GNP of different coatings and the submicron-sized polystyrene particles suggests different protein binding patterns. It is quite surprising that the much higher blood concentration of the 1.4 nm and 5 nm GNP compared to the >18 nm GNP did not lead to an increased uptake in the spleen as was seen in several other organs – see above.

4.6. Hepato-biliary clearance

In the liver, NP – not immediately trapped by Kupffer cells - are translocated through the fenestrated vascular endothelium into the Dissé spaces to be taken up by hepatocytes and processed into biliary canaliculi [46]. From there, they are drained via the biliary duct to the beginning of the small intestine where they become included in the fecal excretion. Concordantly, we found the 18 nm GNP, not only in Kupffer cells, but also in endothelial cells and hepatocytes, highlighting the hepato-biliary pathway. Hepato-biliary clearance of the TPPMS-coated GNP showed an inverse linear relationship to the GNP diameter over the entire size range of 2.8–200 nm; i.e. the smaller the GNP the higher the penetration through the various physiological structures of the liver into the intestine as outlined earlier. The clearance of the carboxylated 2.8 nm GNP fitted very well into this trend of size dependency. The hepato-biliary clearance of the carboxylated 2.8 nm GNP occurred to be about half for negatively charged GNP compared to positively charged GNP which is in line with another study using quantum dots of opposite charges [15]. Only the smallest GNP of 1.4 nm did not follow this linear size relationship, but were cleared with an even higher percentage of 4.6 ± 0.4%. According to this complex pathway, the rate-determining processes are yet to be identified.

5. Conclusion

Size and surface charges of GNP are strong determinants of the biokinetic fate in the organism. The most GNP accumulation was in the liver and the amount increased with the size of GNP. In contrast, there was little size dependency of accumulation of 18 nm to 200 nm GNP in most other organs and in the carcass as well as the blood. But for GNP between 1.4 nm and 5 nm the accumulation increased sharply with decreasing size; the increase was linearly proportional to the volumetric specific surface area of the GNP, i.e. proportional to the inverse of the GNP diameter. The different charges of the 2.8 nm GNP led to significantly different accumulations in most organs, tissues, and body fluids.

From the different accumulation patterns observed as a result of different sized and surface-charged GNP, we conclude that the alterations of the GNP surface area, due to dynamic protein binding and exchange, are major mechanisms determining GNP accumulation in the various organs and tissues. A better understanding of this complex GNP biokinetics is essential for the development of improved drug delivery, as well as for dose estimates of secondary organs and tissues used in risk assessment.

Acknowledgements

We thank Georg Müller (RWTH) for the synthesis and Heidrun Keul (DWI) for the TEM analyses of the 2.8 nm Au particles. We thank Dr. Carsten Rudolph from Dr. von Hauner Children's Hospital, Ludwig-Maximillians-University of Munich, for his support of the zeta-potential measurements. We also thank Dr. Dorothea Alber and Gregor Bukalis from the Helmholtz Zentrum in Berlin for performing the neutron activation of our GNP at the research reactor BER II. This work was partially supported by the German Research Foundation FOR-627, SPP-1313 and PAK 56, the EU-FP6 project Particle-Risk (012912 (NEST)), and the EU FP7 projects NeuroNano (NMP4-SL-2008-214547), ENPRA (NMP4-SL-2009-

228789) as well as InLiveTox (NMP-2008-1.3-2 CP-FP 228625-2) and US-NIH grant HL074022.

References

[1] E. Boisselier, D. Astruc, Gold nanoparticles in nanomedicine: preparations, imaging, diagnostics, therapies and toxicity, Chemical Society Reviews 38 (2009) 1759–1782.
[2] D. Giljohann, D. Seferos, W. Daniel, M. Massich, P. Patel, C. Mirkin, Gold nanoparticles for biology and medicine, Angewandte Chemie International Edition 49 (2010) 3280–3294.
[3] R.A. Sperling, P. Rivera Gil, F. Zhang, M. Zanella, W.J. Parak, Biological applications of gold nanoparticles, Chemical Society Reviews 37 (2008) 1896–1908.
[4] C.D. Medley, J.E. Smith, Z. Tang, Y. Wu, S. Bamrungsap, W.H. Tan, Gold nanoparticle-based colorimetric assay for the direct detection of cancerous cells, Analytical Chemistry 80 (2008) 1067–1072.
[5] R. Bhattacharya, P. Mukherjee, Biological properties of "naked" metal nanoparticles, Advanced Drug Delivery Reviews 60 (2008) 1289–1306.
[6] R. Bhattacharya, C.R. Patra, R. Verma, S. Kumar, P.R. Greipp, P. Mukherjee, Gold nanoparticles inhibit the proliferation of multiple myeloma cells, Advanced Materials 19 (2007) 711–716.
[7] P. Ghosh, G. Han, M. De, C.K. Kim, V.M. Rotello, Gold nanoparticles in delivery applications, Advanced Drug Delivery Reviews 60 (2008) 1307–1315.
[8] C. Lasagna-Reeves, D. Gonzalez-Romero, M.A. Barria, I. Olmedo, A. Clos, V.M.S. Ramanujam, A. Urayama, L. Vergara, M.J. Kogan, C. Soto, Bioaccumulation and toxicity of gold nanoparticles after repeated administration in mice, Biochemical and Biophysical Research Communications 393 (2010) 649–655.
[9] G. Schmid, The relevance of shape and size of Au55 clusters, Chemical Society Reviews 37 (2008) 1909–1930.
[10] O. Bar-Ilan, R.M. Albrecht, V.E. Fako, D.Y. Furgeson, Toxicity assessments of multisized gold and silver nanoparticles in zebrafish embryos, Small 5 (2009) 1897–1910.
[11] Y. Pan, S. Neuss, A. Leifert, M. Fischler, F. Wen, U. Simon, G. Schmid, W. Brandau, W. Jahnen-Dechent, Size-dependent cytotoxicity of gold nanoparticles, Small 3 (2007) 1941–1949.
[12] B.D. Chithrani, A.A. Ghazani, W.C. Chan, Determining the size and shape dependence of gold nanoparticle uptake into mammalian cells, Nano Letters 6 (2006) 662–668.
[13] J.F. Hainfeld, D.N. Slatkin, T.M. Focella, H.M. Smilowitz, Gold nanoparticles: a new X-ray contrast agent, British Journal of Radiology 79 (2006) 248–253.
[14] H.S. Choi, W. Liu, P. Misra, E. Tanaka, J.P. Zimmer, B.I. Ipe, M.G. Bawendi, J.V. Frangioni, Renal clearance of quantum dots, Nature Biotechnology 25 (2007) 1165–1170.
[15] L. Balogh, S.S. Nigavekar, B.M. Nair, W. Lesniak, C. Zhang, L.Y. Sung, M.S.T. Kariapper, A. El-Jawahri, M. Llanes, B. Bolton, F. Mamou, W. Tan, A. Hutson, L. Minc, M.K. Khan, Significant effect of size on the in vivo biodistribution of gold composite nanodevices in mouse tumor models, Nanomedicine-Nanotechnology Biology and Medicine 3 (2007) 281–296.
[16] G. Renaud, R.L. Hamilton, R.J. Havel, Hepatic metabolism of colloidal gold-low-density lipoprotein complexes in the rat: evidence for bulk excretion of lysosomal contents into bile, Hepatology 9 (1989) 380–392.
[17] J.S. Souris, C.H. Lee, S.H. Cheng, C.T. Chen, C.S. Yang, J.A.A. Ho, C.Y. Mou, L.W. Lo, Surface charge-mediated rapid hepatobiliary excretion of mesoporous silica nanoparticles, Biomaterials 31 (2010) 5564–5574.
[18] S.K. Balasubramanian, J. Jittiwat, J. Manikandan, C.N. Ong, L.E. Yu, W.Y. Ong, Biodistribution of gold nanoparticles and gene expression changes in the liver and spleen after intravenous administration in rats, Biomaterials 31 (2010) 2034–2042.
[19] C.T. Kuo, J.Y. Yu, M.J. Huang, C.H. Chen, On the size evolution of gold-monolayer-protected clusters by ligand place-exchange reactions: the effect of headgroup–gold interactions, Langmuir 26 (2010) 6149–6153.
[20] K. Oeff, A. Konig, Blood volume of rat organs and residual amount of blood after blood letting or irrigation; determination with radiophosphorus-labeled erythrocytes, Naunyn-Schmiedebergs Archiv für Experimentelle Pathologie und Pharmakologie 226 (1955) 98–102.
[21] M. Semmler-Behnke, W. Kreyling, J. Lipka, S. Fertsch, A. Wenk, S. Takenaka, G. Schmid, W. Brandau, Biodistribution of 1.4- and 18-nm gold particles in rats, Small 4 (2008) 2108–2111.
[22] W.G. Kreyling, M. Semmler-Behnke, Q. Chaudhry, A complementary definition of nanomaterial, Nano Today 5 (2010) 165–168.
[23] E. Sadauskas, N.R. Jacobsen, G. Danscher, M. Stoltenberg, U. Vogel, A. Larsen, W. Kreyling, H. Wallin, Biodistribution of gold nanoparticles in mouse lung following intratracheal instillation, Chemistry Central Journal 3 (2009).
[24] S. Takenaka, E. Karg, W.G. Kreyling, B. Lentner, W. Moller, M. Behnke-Semmler, L. Jennen, A. Walch, B. Michalke, P. Schramel, J. Heyder, H. Schulz, Distribution pattern of inhaled ultrafine gold particles in the rat lung, Inhalation Toxicology 18 (2006) 733–740.
[25] J. Lipka, M. Semmler-Behnke, R.A. Sperling, A. Wenk, S. Takenaka, C. Schleh, T. Kissel, W.J. Parak, W.G. Kreyling, Biodistribution of PEG-modified gold nanoparticles following intratracheal instillation and intravenous injection, Biomaterials 31 (2010) 6574–6581.
[26] I. Lynch, K.A. Dawson, Protein–nanoparticle interactions, Nano Today 3 (2008) 40–47.
[27] M. Lundqvist, J. Stigler, G. Elia, I. Lynch, T. Cedervall, K.A. Dawson, Nanoparticle size and surface properties determine the protein corona with possible implications for biological impacts, Proceedings of the National Academy of Sciences of the United States of America 105 (2008) 14265–14270.
[28] T. Cedervall, I. Lynch, M. Foy, T. Berggard, S.C. Donnelly, G. Cagney, S. Linse, K.A. Dawson, Detailed identification of plasma proteins adsorbed on copolymer nanoparticles, Angewandte Chemie International Edition England 46 (2007) 5754–5756.
[29] T. Cedervall, I. Lynch, S. Lindman, T. Berggard, E. Thulin, H. Nilsson, K.A. Dawson, S. Linse, Understanding the nanoparticle–protein corona using methods to quantify exchange rates and affinities of proteins for nanoparticles, Proceedings of the National Academy of Sciences of the United States of America 104 (2007) 2050–2055.
[30] H.S. Choi, W.H. Liu, F.B. Liu, K. Nasr, P. Misra, M.G. Bawendi, J.V. Frangioni, Design considerations for tumour-targeted nanoparticles, Nature Nanotechnology 5 (2010) 42–47.
[31] M.A. Dobrovolskaia, A.K. Patri, J.W. Zheng, J.D. Clogston, N. Ayub, P. Aggarwal, B.W. Neun, J.B. Hall, S.E. McNeil, Interaction of colloidal gold nanoparticles with human blood: effects on particle size and analysis of plasma protein binding profiles, Nanomedicine-Nanotechnology Biology and Medicine 5 (2009) 106–117.
[32] A. Gessner, A. Lieske, B.R. Paulke, R.H. Muller, Influence of surface charge density on protein adsorption on polymeric nanoparticles: analysis by two-dimensional electrophoresis, European Journal of Pharmaceutics and Biopharmaceutics 54 (2002) 165–170.
[33] Y. Pan, A. Leifert, D. Ruau, S. Neuss, J. Bornemann, G. Schmid, W. Brandau, U. Simon, W. Jahnen-Dechent, Gold nanoparticles of diameter 1.4 nm trigger necrosis by oxidative stress and mitochondrial damage, Small 5 (2009) 2067–2076.
[34] C.M. Goodman, C.D. McCusker, T. Yilmaz, V.M. Rotello, Toxicity of gold nanoparticles functionalized with cationic and anionic side chains, Bioconjugate Chemistry 15 (2004) 897–900.
[35] B.M. Rothen-Rutishauser, S. Schurch, B. Haenni, N. Kapp, P. Gehr, Interaction of fine particles and nanoparticles with red blood cells visualized with advanced microscopic techniques, Environmental Science and Technology 40 (2006) 4353–4359.
[36] C. Rocker, M. Potzl, F. Zhang, W.J. Parak, G.U. Nienhaus, A quantitative fluorescence study of protein monolayer formation on colloidal nanoparticles, Nature Nanotechnology 4 (2009) 577–580.
[37] M. Geiser, B. Rothen-Rutishauser, N. Kapp, S. Schurch, W. Kreyling, H. Schulz, M. Semmler, V. Im Hof, J. Heyder, P. Gehr, Ultrafine particles cross cellular membranes by nonphagocytic mechanisms in lungs and in cultured cells, Environmental Health Perspectives 113 (2005) 1555–1560.
[38] W.H. De Jong, W.I. Hagens, P. Krystek, M.C. Burger, A.J. Sips, R.E. Geertsma, Particle size-dependent organ distribution of gold nanoparticles after intravenous administration, Biomaterials 29 (2008) 1912–1919.
[39] G.S. Terentyuk, G.N. Maslyakova, L.V. Suleymanova, B.N. Khlebtsov, B.Y. Kogan, G.G. Akchurin, A.V. Shantrocha, I.L. Maksimova, N.G. Khlebtsov, V.V. Tuchin, Circulation and distribution of gold nanoparticles and induced alterations of tissue morphology at intravenous particle delivery, Journal of Biophotonics 2 (2009) 292–302.
[40] N.-E. Säterborg, The distribution of ^{198}Au injected intravenously as a colloid and in solution, Acta Oncologica 12 (1973) 509–528.
[41] G. Sonavane, K. Tomoda, K. Makino, Biodistribution of colloidal gold nanoparticles after intravenous administration: effect of particle size, Colloids and Surfaces B – Biointerfaces 66 (2008) 274–280.
[42] W.G. Kreyling, M. Semmler, F. Erbe, P. Mayer, S. Takenaka, G. Oberdörster, A. Ziesenis, Minute translocation of inhaled ultrafine insoluble iridium particles from lung epithelium to extrapulmonary tissues, Annals of Occupational Hygiene 46 (2002) 223–226.
[43] M. Semmler, J. Seitz, F. Erbe, P. Mayer, J. Heyder, G. Oberdorster, W.G. Kreyling, Long-term clearance kinetics of inhaled ultrafine insoluble iridium particles from the rat lung, including transient translocation into secondary organs, Inhalation Toxicology 16 (2004) 453–459.
[44] W.G. Kreyling, M. Semmler-Behnke, J. Seitz, W. Scymczak, A. Wenk, P. Mayer, S. Takenaka, G. Oberdorster, Size dependence of the translocation of inhaled iridium and carbon nanoparticle aggregates from the lung of rats to the blood and secondary target organs, Inhalation Toxicology 21 (2009) 55–60.
[45] S.M. Moghimi, C.J.H. Porter, I.S. Muir, L. Illum, S.S. Davis, Non-phagocytic uptake of intravenously injected microspheres in rat spleen – influence of particle-size and hydrophilic coating, Biochemical and Biophysical Research Communications 177 (1991) 861–866.
[46] H.J. Johnston, G. Hutchison, F.M. Christensen, S. Peters, S. Hankin, V. Stone, A review of the in vivo and in vitro toxicity of silver and gold particulates: particle attributes and biological mechanisms responsible for the observed toxicity, Critical Reviews in Toxicology 40 (2010) 328–346.
[47] T. Tominaga, S. Tenma, H. Watanabe, U. Giebel, G. Schmid, Tracer diffusion of a ligand-stabilized two-shell gold cluster, Chemistry Letters (1996) 1033–1034.

6.2 Size and surface charge of gold nanoparticles determine absorption across intestinal barriers and accumulation in secondary target organs after oral administration

Nanotoxicology, February 2012; 6(1): 36–46

informa
healthcare

Size and surface charge of gold nanoparticles determine absorption across intestinal barriers and accumulation in secondary target organs after oral administration

CARSTEN SCHLEH[1], MANUELA SEMMLER-BEHNKE[1], JENS LIPKA[1], ALEXANDER WENK[1], STEPHANIE HIRN[1], MARTIN SCHÄFFLER[1], GÜNTER SCHMID[2], ULRICH SIMON[3], & WOLFGANG G. KREYLING[1]

[1]*Comprehensive Pneumology Center – Institute of Lung Biology and Disease and Focus Network NP and Health, Helmholtz Zentrum München – German Research Center for Environmental Health, Neuherberg, Germany,* [2]*Institute of Inorganic Chemistry, University Duisburg-Essen, Essen, Germany, and* [3]*Institute of Inorganic Chemistry, RWTH Aachen University, Aachen, Germany*

(Received 27 September 2010; accepted 4 January 2011)

Abstract

It is of urgent need to identify the exact physico-chemical characteristics which allow maximum uptake and accumulation in secondary target organs of nanoparticulate drug delivery systems after oral ingestion. We administered radiolabelled gold nanoparticles in different sizes (1.4–200 nm) with negative surface charge and 2.8 nm nanoparticles with opposite surface charges by intra-oesophageal instillation into healthy adult female rats. The quantitative amount of the particles in organs, tissues and excrements was measured after 24 h by gamma-spectroscopy. The highest accumulation in secondary organs was mostly found for 1.4 nm particles; the negatively charged particles were accumulated mostly more than positively charged particles. Importantly, 18 nm particles show a higher accumulation in brain and heart compared to other sized particles. No general rule accumulation can be made so far. Therefore, specialized drug delivery systems via the oral route have to be individually designed, depending on the respective target organ.

Keywords: *Gold NP, gavage, absorption, gastro-intestinal tract,* in vivo *biodistribution*

Introduction

Nanoparticulate drug delivery systems are very promising. An ideal nanodelivery system would allow high drug load, maximum absorption and specific targeting of the drug combined with minimal side-effects. Besides biodegradable nanoparticles (NPs) like solid lipid NPs (Nassimi et al. 2009, 2010) or polymer-based NPs (Bhardwaj et al. 2009), gold (Au) NPs are also discussed. They can be easily and precisely synthesized and exactly detected by transmission electron microscopy (TEM) due to their high electron density. In addition, several target molecules can get attached to them (Sperling et al. 2008). Importantly, gold NPs seem to exhibit a low cytotoxicity (Connor et al. 2005). However, it is important to note that cytotoxicity is strongly dependent on the exact nature of the gold NPs. Very small Au-cluster, e.g., fit into the grooves of DNA-molecules (Schmid 2008), induce oxidative stress (Pan et al. 2009), and thereby cause cytotoxic effects. Nowadays, several gold NP-based drugs are investigated and clinical trials are under development.

Drugs can be administered via several pathways. Thereby the intravenous injection, the inhalation as well as the ingestion are the most prominent. From these, the oral route is the most convenient route since it is non-invasive and widely accepted by most of the patients.

However, little is known about the uptake of NPs across the gastro-intestinal membranes and the following accumulation in secondary target organs. In particular it is known that general uptake of particles into single cells may be dependent on size (Geiser et al. 2005) and surface charge (He et al. 2010) of the particles. It is generally believed that absorption

Correspondence: Dr Carsten Schleh, PhD, Comprehensive Pneumology Center, Helmholtz Zentrum München, Insitute of Lung Biology and Disease, Ingolstädter Landstraße 1, 85764 Neuherberg, Germany. Tel: +49 0 89 3187 2673. Fax: +49 0 89 3187 3397. E-mail: carsten.schleh@helmholtz-muenchen.de

ISSN 1743-5390 print/ISSN 1743-5404 online
DOI: 10.3109/17435390.2011.552811

across the intestinal membrane to the circulation is somehow dependent on size (Florence et al. 1995; Powell et al. 2010; Ruenraroengsak et al. 2010). Although several studies exist describing the uptake of NPs in *in vitro* systems, only a small number of papers focus on the guidance of nanosystems to biological targets which is an urgent need in pharmaceutical research (Florence 2007). As far as we know, no 100% quantitative biodistribution study comparing NPs with different sizes and surface charge after oral ingestion exists.

Thereby, the aim of the present study was to consider the physico-chemical characteristics which determine the absorption across intestinal membranes as well as the accumulation in secondary target organs. Therefore, gold NPs as model particles for drug delivery, in five different sizes (1.4, 5, 15, 80 and 200 nm) as well as opposite surface charges (positive and negative) at equal size (2.8 nm) were applied by intra-oesophageal instillation in healthy adult female rats. A 100% biodistribution of the applied NPs was investigated after 24 h. As far as we know, this is the first study describing the precise quantitative absorption and accumulation of NPs in secondary target organs after oral ingestion.

Materials and methods

Animal housing

Healthy, female Wistar-Kyoto rats (WKY/Kyo@Rj rats, Janvier, Le Genest Saint Isle, France), 8–10 weeks of age (approx. 250 g body weight) were housed in pairs in humidity and temperature-controlled ventilated cages (VentiRack Bioscreen TM, Biozone, Margate, UK) on a 12-h day/night cycle. Rodent diet and water were provided *ad libitum*. All experiments were conducted under German federal guidelines for the use and care of laboratory animals and were approved by the Regierung von Oberbayern (Government of District of Upper Bavaria, Approval No. 211-2531-94/04) and by the Institutional Animal Care and Use Committee of Helmholtz Center Munich.

NP preparation and characterization

Mono-sulfonated triphenylphosphine (TPPMS) stabilized Gold NP (Table I) (1.4 and 18 nm) were synthesized following known procedures (Pan et al. 2007). Citrate stabilized gold NPs (5, 80 and 200 nm) were provided from Plano (Wetzlar, Germany). Ligand exchange (citrate to TPPMS) was accomplished as described previously (Pan et al. 2007).

Table I. Characteristics of the applied ^{198}Au NP suspensions.

	1.4 nm	5 nm	18 nm	80 nm	200 nm	2.8 nm Carboxyl	2.8 nm Amine
Applied radioactivity [kBq]	76.0 ± 33.3	130.2 ± 10.3	73.5 ± 2.3	297.1 ± 5.1	219.5 ± 2.	21.8 ± 0.1	90.6 ± 5.8
Applied mass [µg]	1.0 ± 0.5	27.4 ± 2.2	2.4 ± 0.1	19.9 ± 0.3	19.0 ± 0.2	1.4 ± 0.1	16.4 ± 1.1
Applied number	$3.8 \pm 1.7 \times 10^{13}$	$2.2 \pm 0.2 \times 10^{13}$	$4.1 \pm 0.1 \times 10^{10}$	$3.9 \pm 0.1 \times 10^{9}$	$3.8 \pm 0.0 \times 10^{8}$	$6.3 \pm 0.2 \times 10^{12}$	$7.5 \pm 0.5 \times 10^{13}$
Applied surface area [cm^2]	2.4 ± 1.0	17.3 ± 1.4	0.4 ± 0.0	0.8 ± 0.0	0.1 ± 0.0	1.2 ± 0.1	14.5 ± 1.0

The fabrication of the 2.8 nm gold particles followed the same procedure as described in Pan et al. (2007) by performing ligand exchange of initially 1.4 nm Au particles stabilized with triphenylphosphine (TPP). Via phase transfer from a dichloromethane phase to an aqueous phase TPP is replaced by thioglycolic acid (TGA) for negatively charged particles and by cysteamine (CA) for positively charged particles, respectively. The driving force for this exchange reaction is the higher binding affinity of thiol groups to gold compared to phosphine groups accompanied with the change in polarity, since the particles pass from the dichloromethane phase into the aqueous phase, when TPP is replaced by TGA or CA, respectively. Hence, the solubility of the particles in water gives immediate evidence that the ligand exchange was successful.

As already been observed by others, the replacement of TPP by thiol ligands is associated with a growth of the gold core (Balasubramanian et al. 2005; Kuo et al. 2010). This holds for our ligand exchange procedure as well, where the introduction of thiol ligands TGA and CA resulted in an increase of the mean core particle size, which was determined by TEM analyses to be 2.8 ± 0.4 nm for both ligands.

All Au NP were activated by neutron irradiation (^{197}Au (n,) ^{198}Au). For this, the NPs were activated at a neutron flux of 10^{14} cm^{-2} s^{-1} at the research reactor of the Helmholtz Center Berlin (formerly Hahn-Meitner Institute), Berlin, Germany. Gold amounts and irradiation times were adjusted to provide sufficient ^{198}Au radioactivity for the subsequent *in vivo* studies.

After neutron irradiation immediately prior to rat application, the 1.4 nm and the 2.8 nm ^{198}Au-NP solution was filtered through a 10 cm column of Celite to remove agglomerates; losses determined by ^{198}Au radioactivity accounted for about 10%. All other ^{198}Au-NP suspensions from 5–200 nm were visually controlled for precipitates and their correct pink translucent color of the colloidal suspension immediately prior to the application in rats; no changes were found compared to the suspension prior to irradiation.

Zeta-potential measurements were performed in triplicate using appropriate working dilutions in a Zetapalssystem (Brookhaven Instruments Corporation, Holtsville). Hydrodynamic diameters were measured in triplicate using appropriate working dilutions in a Malvern HPPS5001 or a Malvern Zetasizer (Malvern, Herrenberg, Germany).

NP administration and animal maintenance in metabolic cages

NP suspensions were applied to non-fasted animals by intra-oesophageal instillation. We applied low concentrations of NP (1–27 μg) to avoid toxic reactions in the gastro-intestinal tract (GIT) in order to maintain a healthy intestinal barrier capacity. For this purpose rats were anesthetized by inhalation of 5% isoflurane until muscular tonus relaxed. The anesthetized rat was fixed with its incisors to a rubber band on a board at an angle of 60° to the lab bench. A flexible cannula (2.7 × 50 mm, B. Braun, Melsungen, Germany) was placed into the upper third of the oesophagus and the suspension (50 μl) which contained NP (Table II) was gently instilled. After administration of the NP suspensions, rats were kept individually in metabolism cages (Tecniplast, Hohenpreissenberg, Germany) for separate collection of urine and feces.

Sample preparation

Twenty-four hours after administration, rats were anesthetized (5% isoflurane inhalation) and

Table II. Characteristics of the applied gold NPs.

Core diameter [nm]	Hydrodynamic diameter [nm]	Polydispersity Index (PdI)	Ligand (Charged surface group)	ζ-potential [mV]
1.4	2.9*	ND	TPPMS (SO_3^-)	−20.6 ± 0.5
5	12.1[#]	0.19	TPPMS (SO_3^-)	−21.1 ± 1.4
18	21[§]	0.10	TPPMS (SO_3^-)	−22.8 ± 3.1
80	85[#]	0.12	TPPMS (SO_3^-)	−22.3 ± 1.6
200	205[#]	0.05	TPPMS (SO_3^-)	−41.3 ± 4.5
2.8	ND	ND	TGA (COO^-)	Negative
2.8	ND	ND	CA (NH_3^+)	Positive

*As determined earlier (Tominaga et al. 1996); [#]DLS measurement using Malvern HPPS5001, Herrenberg, Germany; [§]DLS measurement using Malvern Zetasizer, Herrenberg, Germany. TPPMS, triphenylphosphine m-monosulfonate; TGA, thioglycolic acid (mercaptoacetic acid); CA, cysteamine (2-aminoethanethiol); ND, Not determined.

euthanized by exsanguination via the abdominal aorta. Approximately 70% of the total blood volume was withdrawn. For radioanalysis, organs and tissues listed below as well as total excretion and the entire remaining carcass were collected.

- *Organs*: Lungs, liver, spleen, kidneys, brain, heart, exsanguinated blood; gastro-intestinal tract: oesophagus, stomach, small and large intestine; Remainder: total remaining carcass beyond the listed organs;
- *Excretion*: Total urine and feces, collected separately.
- While dissecting, no organs were cut and all fluids were cannulated where necessary in order to avoid any cross contamination.

Radioanalysis

The ^{198}Au radioactivity of all samples were measured by γ-spectroscopy without any further physico-chemical preparation in either a lead-shielded 10 ml or a lead-shielded 1 l well type NaI (Tl) scintillation detector. The count rates were corrected for physical decay and background radiation. Additionally, count rates were calibrated to a ^{198}Au reference source in order to correlate ^{198}Au radioactivities to the numbers and masses of the Au NPs. Samples yielding net counts (i.e., background-corrected counts) less than three standard deviations of the totally measured counts in the photo-peak region-of-interest of the ^{198}Au gamma spectrum were defined as below the detection limit. For a complete balance of the administered ^{198}Au radioactivity within each rat ^{198}Au radioactivities of all samples were summed up for each rat and used as a denominator for the calculation of the ^{198}Au percentage of each sample.

Blood correction

Blood contents of organs and tissues were calculated according to the findings of Oeff and Konig (1955). The NP content of the remaining blood volume of each sample was estimated and subtracted from the measured ^{198}Au radioactivity to maintain the absolute ^{198}Au activity of the tissue or organ. In the case of the carcass, the difference between the estimated total blood volume of the animal and the sum of all organ blood contents and the collected blood sample was calculated to be the blood volume of the carcass.

Calculations and statistical analysis

Four animals per group were used. Calculated values are given as a percentage of the relevant integral ^{198}Au radioactivity (calculated for a reference date) of all samples in each animal with the standard error of the mean (SEM). All radioactivities were correlated with the corresponding mass of gold NPs in each animal. All calculated significances are based on a one-way ANOVA test and a post hoc Tukey test. In the case of an individual two group comparison, the unpaired *t*-test was used; $p \leq 0.05$ was accounted for significance.

Results

Effect of surface charge of 2.8 nm gold NP

Absorption to the circulation. After 24 h, most of the applied 2.8 nm gold NPs were found in the GIT as well as in feces (Table III), indicating that intestinal passage and excretion was not complete within 24 h. For most of the particles, no absorption to the circulation took place. However, surface charge is

Table III. NP content in the gastro-intestinal tract (GIT).

	Particle retention [%]		
Particle type	GIT with internal feces	Excreted feces	GIT+feces
1.4 nm	17.2 ± 4.0	82.4 ± 4.0	99.63 ± 0.10
5 nm	74.1 ± 14.0	25.9 ± 14.0	99.95 ± 0.01
18 nm	29.7 ± 6.7	70.3 ± 6.7	99.88 ± 0.02
80 nm	22.3 ± 7.3	77.7 ± 7.3	99.97 ± 0.01
200 nm	34.9 ± 7.1	65.1 ± 7.1	99.99 ± 0.00
2.8 nm COO^-	54.2 ± 4.5	45.4 ± 4.5	99.63 ± 0.02
2.8 nm NH_3^+	64.8 ± 11.8	35.0 ± 11.8	99.86 ± 0.02

NP content in the gastro-intestinal tract (including internal feces) and excreted feces after intra-oesophageal application in % of administered particle-amount.

important for the absorption across intestinal membranes (Figure 1). Significantly more negatively charged 2.8 nm (TGA ligand with carboxyl-groups) NPs absorbed compared to positive 2.8 nm particles (CA ligands with amine-groups). Therefore values of 0.37 ± 0.02% and 0.14 ± 0.02%, respectively, were detected.

Distribution in the body and accumulation in secondary target organs. 2.8 nm gold NPs were found in nearly all organs, tissues, blood and urine. Most importantly, in the liver, the urine, as well as the remainder, the negatively charged particles accumulated to a higher amount compared to the positively charged particles ($p < 0.05$). The highest accumulation of particles was found in the remaining carcass, where 0.21 ± 0.01% of the applied negative particles and 0.06 ± 0.02% of the applied positive particles were detected (Figure 2A). Interestingly, no negative charged 2.8 nm particles could be found in the brain (detection limit 10^{-5} of administered dose). In contrast, a low but detectable amount of $2.0 \pm 0.7 \times 10^{-4}$ % of the applied positively charged particles were detected in the brain (Figure 2B).

Effect of particle size between 1.4 and 200 nm of TPPMS-coated gold NP

Absorption to the circulation. The highest absorption across intestinal membranes was found for the smallest particles (Figure 3). Thereby after 24 h, 0.37 ± 0.10% of the applied 1.4 nm particles reached the circulation. Importantly, a larger size of the particles led to a lower amount of absorbed particles. Therefore, 0.05 ± 0.01% of the 5 nm particles, 0.03 ± 0.01% of the 80 nm particles, as well as 0.01 ± 0.00% of the 200 nm particles reached the circulation after 24 h. To our surprise, 0.12 ± 0.02% of the 18 nm particles reached the circulation and hence more than the lower sized 5 nm particles.

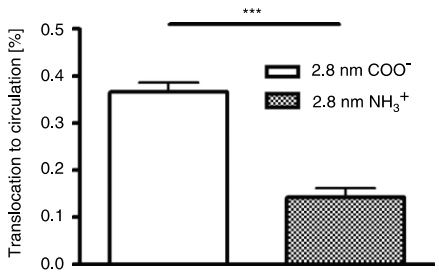

Figure 1. NP content which reached the circulation after intra-oesophageal application in % of administered particle-amount. Given is the mean ± standard error of the mean of four animals.
***$p < 0.001$.

Distribution in the body and accumulation in secondary target organs. As for the absorption across the intestinal membranes, the accumulation in blood, kidneys, parts of the reticulo-endothelial-system (liver and spleen; RES), as well as the urine was mostly dependent on the size of the particles. In blood 0.07 ± 0.02% of the applied 1.4 nm particles were found 24 h after application (Figure 4A) which is a significantly higher amount than for all larger sized particles. Again, the 18 nm particles showed the second highest retention with 0.02 ± 0.01% of the applied NPs. The highest amount of accumulated particles in the RES, the kidneys, as well as the urine was detected for the 1.4 nm particles, too (Figure 4B, C, D); i.e., 0.02 ± 0.01%, 0.05 ± 0.01%, as well as 0.06 ± 0.02% of the applied particles, respectivelyly. Again, significantly lower amounts of the larger sized particles were detected. Surprisingly, the highest amount of accumulated particles in the heart and the brain was measured for the 18 nm particles – even more than for the 1.4 nm particles. In detail, $1.5 \pm 0.4 \times 10^{-3}$ % and $1.6 \pm 0.4 \times 10^{-3}$ % of the applied 18 nm particles were detected in these organs (Figure 5). In the brain, only $3.1 \pm 1.9 \times 10^{-4}$ % of the 1.4 nm particles, $8.3 \pm 8.3 \times 10^{-5}$ % of the 5 nm particles, and $1.3 \pm 0.7 \times 10^{-4}$ % of the 80 nm particles accumulated (Figure 4B). These are significantly lower amounts compared to the amount of accumulated 18 nm particles. No 200 nm particles were detected. The highest amount of the applied particles was detected in the remaining carcass, which incorporates adipose tissue, bones, muscles and skin (Figure 6). 0.17 ± 0.04% of the 1.4 nm particles, 0.02 ± 0.00% of the 5 nm particles, 0.08 ± 0.01% of the 18 nm particles, 0.02 ± 0.01% of the 80 nm particles, and 0.01 ± 0.00% of the 200 nm particles were detected.

Effect of different NP-doses. To clarify, whether different doses of administered NPs have any effect on the absorption as well as accumulation in secondary target organs, we administered in an additional experiment beside the 1.0 µg of the 1.4 nm NPs also 22.3 µg of the 1.4 nm NPs. Importantly, there was no statistically significant difference in absorption or accumulation in single organs after comparing the two different doses with *t*-test (data not shown).

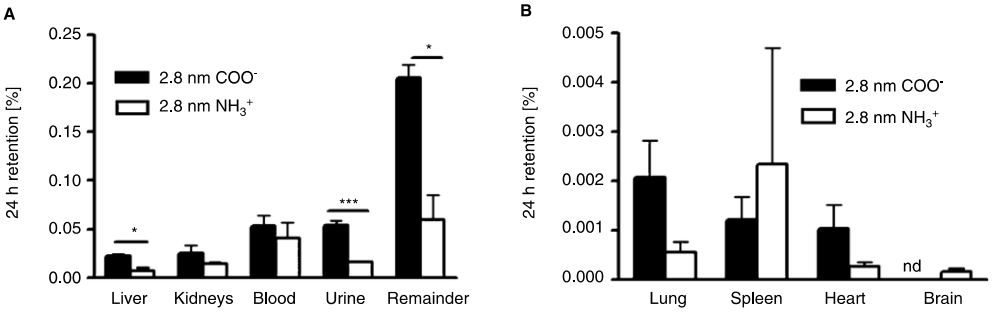

Figure 2. NP content which accumulated in secondary organs, the remainder, as well as the urine after intra-oesophageal application in % of administered particle-amount. Given is the mean ± standard error of the mean of four animals. *$p < 0.05$; ***$p < 0.001$; nd, not detected.

Discussion

In the present manuscript we investigated the absorption of NP across intestinal barriers as well as the subsequent accumulation in secondary target organs. Importantly, by using gamma-spectroscopy we were able to measure all NPs in the entire organism and total excretion of each rat as well as in each syringe and cannula we used for the application. We detected little but variable losses during the procedure of application of the prepared NP suspensions and hence we were able to accurately determine the administered NP dose which really reached the animal. Furthermore, we quantitatively determined the entire NP dose in the entire animal by analyzing each organ and tissue and total excretion in a 100% balance of the biodistribution of the applied NP. Importantly, the ^{198}Au sum of all samples after 24 h (corrected for radioactive decay) was counterchecked to be the same as the ^{198}Au value of the initially prepared NP suspensions minus the losses during application.

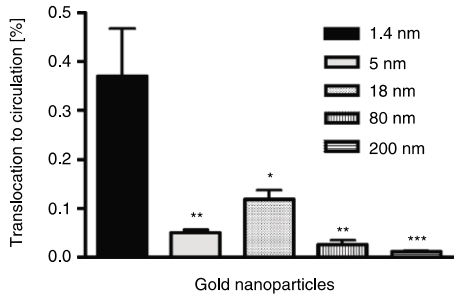

Figure 3. NP content which reached the circulation after intra-oesophageal application in % of administered particle-amount. Given is the mean ± standard error of the mean of four animals. *$p < 0.05$ vs 1.4 nm; **$p < 0.01$ vs. 1.4 nm; ***$p < 0.001$ vs 1.4 nm.

We showed that absorption of NPs across intestinal membranes and the consequent accumulation in secondary organs is to a large part dependent on the size and surface charge of the particles. Thereby, a smaller size and a negative charge generally led to a higher absorption and further accumulation. Importantly, 18 nm particles were absorbed across intestinal barriers and accumulated in specific secondary organs to a higher amount than smaller particles.

Absorption to the circulation

Several pathways are possible for absorption of particles across intestinal barriers and the most relevant are the paracellular transport and the transcellular transport. Paracellular transport is mainly limited by tight junctions, which seal the cell-cell contacts. However, it is known that small molecules can pass the tight junctions and the pore-diameter which allows penetration is variously quoted around 0.6–5 nm (Ruenraroengsak et al. 2010). In addition, dendritic cells are able to open tight junctions and to send processes to the lumen where they may take up NPs (Rimoldi and Rescigno 2005). Transcytosis may appear across enterocytes or M-cells. However, since the endocytic activity of enterocytes is limited compared to M-cells (des Rieux et al. 2006) we conclude, that enterocytes probably do not play a big role in absorption of NPs in particular, since it is also known that NP diffusion across enterocytes only happens to a small extent, too (Cartiera et al. 2009). Therefore, the most prominent cells, which exhibit a high transcytotic activity, are the M-cells located in the Peyer's patches (Sass et al. 1990; Seifert and Sass 1990; Gebert et al. 1996; Seifert et al. 1996). A third additional mechanism, which is between paracellular and transcellular transport, is the transport of the particles across degrading enterocytes. Hillyer and Albrecht (2001) investigated a high occurence of gold NPs

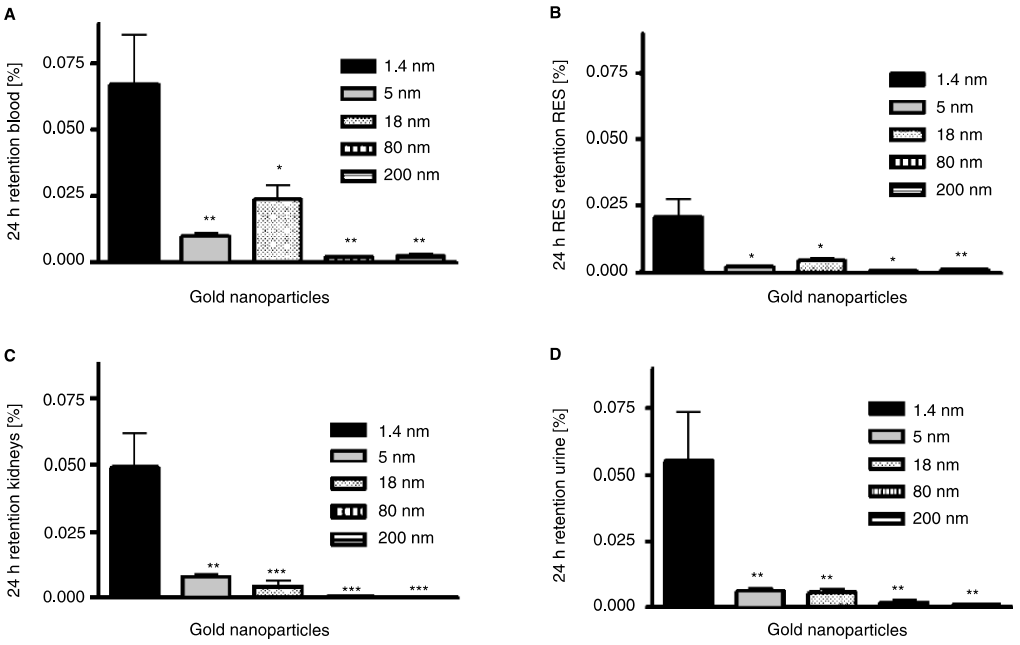

Figure 4. NP content which accumulated the blood (A), reticulo endothelial system (RES; liver plus spleen), (B), kidney (C), as well as urine (D) after intra-oesophageal application in % of administered particle-amount. Given is the mean ± standard error of the mean of four animals. *$p < 0.05$ vs 1.4 nm; **$p < 0.01$ vs. 1.4 nm; ***$p < 0.001$

in degrading enterocytes – the lower the size of the particles was, the higher was the occurrence of particles inside the cells. Since it is known, that approximately 2×10^8 (mice) – 10^{11} (men) enterocytes are shed per day in the small intestine (Potten and Loeffler 1990), this is a reasonable pathway for our gold NPs. However, since the aim of this study was the investigation of the 100% quantitative biodistribution in all secondary target organs and not the detailed identification of potential uptake mechanisms, we have not proven this by electron microscopy. We speculate that the 1.4 nm particles enter the circulation by both mechanisms, transcelluar as well as paracellular across tight junctions. Furthermore, we hypothesize that the bigger sized particles (5–200 nm) are too large for paracelluar mechanisms, which may explain that the amount of transcloated 1.4 nm particles is at least three-fold higher than for

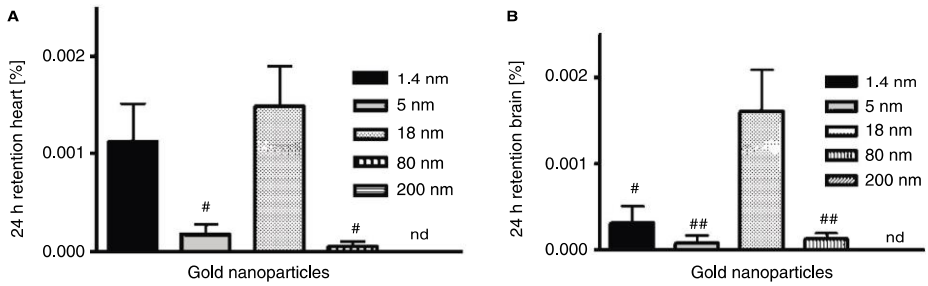

Figure 5. NP content which accumulated the heart (A), and brain (B) after intra-oesophageal application in % of administered particle-amount. Given is the mean ± standard error of the mean of four animals.
#$p < 0.05$ vs. 18 nm; ##$p < 0.01$ vs. 18 nm; nd, not detected.

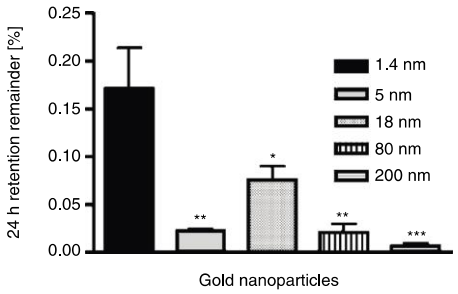

Figure 6. NP content which accumulated in the remaining carcass after intra-oesophageal application in % of administered particle-amount. Given is the mean ± standard error of the mean of four animals.
*$p < 0.05$ vs. 1.4 nm; **$p < 0.01$ vs. 1.4 nm; ***$p < 0.001$ vs. 1.4 nm.

the other sizes. The larger sized particles are probably absorbed exclusively by transcytosis across M-cells. Consistently, since it is generally believed that smaller particles are absorbed to a higher degree than larger particles (Jani et al. 1990; Hillyer and Albrecht 2001; Sonavane et al. 2008; Ruenraroengsak et al. 2010), this agrees with a large part of our results.

It is important to note that the different applied mass doses are most probably not responsible for any absorption or accumulation effect as described in this manuscript. In addition to the 1.0 μg mass dose for the 1.4 nm NPs, we administered an approximately 20 times higher dose of these particles. Thereby we wanted to prove if this difference in mass has any effect regarding the absorption and biodistribution of the NPs. There was no statistically significant difference in absorption or accumulation in single organs after comparing the two different doses with *t*-test. Thereby we conclude that the different doses used in this study are not responsible for any of the significant differences as described in the present manuscript.

It is important to note that we used a short 2 min isoflurane anesthesia during the gavage and it is known that this may lead to a little decrease in gastrointestinal function (Torjman et al. 2005). However, this report described that after an approximately 6-min isoflurane anesthesia, a significant impact is given after 120 min. Since we used just a very short 2 min anesthesia and since we investigated the biodistribution after a much longer time point than 120 min, we do not think that this very short anesthesia has any big input on our results. In addition, we used the same isoflurane anesthesia for each group which would lead to a little intestinal disturbance in each of the groups which thereby leads to a comparability among the different NP-sizes and charges.

To try to explain the higher absorption and accumulation of the 18 nm gold particles compared to even smaller particles, one has to consider possible protein coatings. In the stomach, the acidic environment as well as the gastrointestinal enzymes are likely to degrade the surface coatings of the NPs. In particular it is known that the triphenylphosphine layer on the surface of the gold NPs used is easily degraded in biological systems, a process, which is less likely for the stronger binding thiols, such as TGA or GA (Pan et al. 2009). Thereby, protein coating of the blank surface of the NPs may occur (Lundqvist et al. 2008; Aggarwal et al. 2009; Dobrovolskaia et al. 2009; Lacerda et al. 2010), which would most probably happen in the less acidic small bowel lumen. This so-called protein corona would hide the particle inside and is thereby mostly responsible for interaction with the intestinal barriers (Walczyk et al. 2010). Transport of the protein across the intestinal epithelium could thereby lead to incidental absorption of the NPs inside, sufficient circulation time in blood and accumulation in secondary organs resulting for instance, in the enhanced accumulation of 18 nm NPs in the brain (Trojan horse effect). Importantly, protein adsorption on NPs is able to change the structure and function of the protein or may preferentially select some proteins over others, which is in detail dependent on the curvature of the particle surface (Lundqvist et al. 2004; Vertegel et al. 2004; Asuri et al. 2006; Shang et al. 2009). Therefore we hypothesize that the specific curvature and surface structure of the 18 nm particles alters the stucture and function of single adsorbed proteins or selects proteins with an increased epithelial penetration probability compared to the other NPs used. Thereby, a specific increased absorption across intestinal membranes occurs. Importantly, a study from our laboratory with exactly the same NPs, injected into the tail vein of rats (Hirn et al. 2010), showed no special modulation of organ accumulations of the 18 nm NPs as seen in the present manuscript. This supports our interpretation that special intestinal incidents are responsible for these results. This has to be further investigated in the future.

Importantly, after protein binding, the physicochemical characteristics of the NP surface may change. Therefore, due to the adsorbed proteins, a positively-charged particle could obtain a negative surface charge and vice versa. We hypothesize that in our experiments the surface charge was altered due to adsorbed proteins. Since it is known that positively-charged particles exhibit a higher absorption in the gastro-intestinal-tract (GIT) (Jani et al. 1989; des Rieux et al. 2005; Hariharan et al. 2006),

this would explain why initially negative-charged particles absorb to a higher amount across the intestinal membranes than initially positive-charged particles.

A comparison of our investigated amount of translocated NPs to the circulation with the literature is difficult. Several studies focused on the uptake of particles in specific cells or regions of the GIT (Hillery et al. 1994; Doyle-McCullough et al. 2007; Smyth et al. 2008). However, only few studies investigated the absorption beyond the intestinal barriers *in vivo* and a comparable quantitative 100% biodistribution study of absorbed NPs is missing at all. Hussain and Florence (1998) have shown, for instance, that more than 10% of administered 500 nm latex particles could be found in the circulaton of rats 24 h later. Even though no 100% biodistribution analysis was conducted in a study of Florence et al. (2000), less than 1% absorption after 24 h can be estimated for 1.8 nm dendrimers, since most of the important organs were investigated. It is important to note that in our study the amount of NPs taken up across the intestinal barriers after 24 h could be even higher than investigated. It is known that NPs may leave the circulation by biliary clearance (Jani et al. 1996; Cho et al. 2009). These particles would therefore re-enter the GIT and thereby add to the amount of particles in the GIT which did not translocate – although they already entered the circulation. However, since the biliary clearance of NPs is rather low (Semmler-Behnke et al. 2008; Hirn et al. 2010), this should not significantly alter the results of the present study.

In the present study, we found that the total absorption of NPs to the circulation is rather low during 24 h. Thereby, the application of these gold NPs as carriers for drug delivery appears not immediately promising as a significant amount of drugs would hardly reach the circulation or special secondary organs. However, besides designing the optimal particles with regard to size and surface charge, the uptake of the drug-loaded particles can be further modulated. One example is the co-administration of other molecules or substances. These substances could enhance absorption of the NPs. For example, it is known that bile salts are able to enhance the oral delivery of PLGA NPs (Samstein et al. 2008). However, it has to be tested if co-administration of substances influences the accumulation in secondary organs, too.

In summary, we have shown that the highest absorption across intestinal barriers were found for 1.4 nm gold particles, whereas for the 2.8 nm particles the negative charge is favoured over positive charge. However, size and surface charge are not responsible alone, since 18 nm particles are absorbed more than 5 nm particles and they have the highest accumulation in the brain which is probably due to selected protein binding. Thereby we conclude that particulate drug delivery systems have to be designed individually – depending on the respective target organ.

Acknowledgements

We thank Georg Müller (RWTH) for the synthesis and Heidrum Keul (DWI) for the TEM analyses of the 2.8 nm Au particles. We thank Dr Carsten Rudolph from Dr von Hauner Children's Hospital, LMU Munich, for his supports of zeta potential measurements. We also thank Dr Dorothea Alber and Gregor Bukalis from the Helmholtz Zentrum in Berlin for performing the neutron activation of our GNP at the research reactor BER II.

Declaration of interest: This work was partially supported by the German Research Foundation FOR 627, SPP 1313 and PAK 56, the EU-FP6 project Particle-Risk (012912 (NEST)), and the EU FP7 projects NeuroNano (NMP4-SL- 2008-214547), ENPRA (NMP4-SL-2009-228789) as well as InLIveTox (NMP-2008-1.3-2 CP-FP 228625-2) and US-NIH grant HL074022. The authors report no conflict of interest. The authors alone are responsible for the content and writing of the paper.

References

Aggarwal P, Hall JB, McLeland CB, Dobrovolskaia MA, McNeil SE. 2009. Nanoparticle interaction with plasma proteins as it relates to particle biodistribution, biocompatibility and therapeutic efficacy. Adv Drug Deliv Rev 61(6): 428–437.

Asuri P, Karajanagi SS, Yang H, Yim TJ, Kane RS, Dordick JS. 2006. Increasing protein stability through control of the nanoscale environment. Langmuir 22(13):5833–5836.

Balasubramanian R, Guo R, Mills AJ, Murray RW. 2005. Reaction of Au(55)(PPh(3))(12)Cl(6) with thiols yields thiolate monolayer protected Au(75) clusters. J Am Chem Soc 127(22): 8126–8132.

Bhardwaj V, Ankola DD, Gupta SC, Schneider M, Lehr CM, Kumar MN. 2009. PLGA nanoparticles stabilized with cationic surfactant: Safety studies and application in oral delivery of paclitaxel to treat chemical-induced breast cancer in rat. Pharm Res 26(11):2495–2503.

Cartiera MS, Johnson KM, Rajendran V, Caplan MJ, Saltzman WM. 2009. The uptake and intracellular fate of PLGA nanoparticles in epithelial cells. Biomaterials 30 (14):2790–2798.

Cho M, Cho WS, Choi M, Kim SJ, Han BS, Kim SH, Kim HO, Sheen YY, Jeong J. 2009. The impact of size on tissue distribution and elimination by single intravenous injection of silica nanoparticles. Toxicol Lett 189(3):177–183.

Connor EE, Mwamuka J, Gole A, Murphy CJ, Wyatt MD. 2005. Gold nanoparticles are taken up by human cells but do not cause acute cytotoxicity. Small 1(3):325–327.

des Rieux A, Fievez V, Garinot M, Schneider YJ, Preat V. 2006. Nanoparticles as potential oral delivery systems of proteins and vaccines: A mechanistic approach. J Control Release 116(1):1–27.

des Rieux A, Ragnarsson EG, Gullberg E, Preat V, Schneider YJ, Artursson P. 2005. Transport of nanoparticles across an in vitro model of the human intestinal follicle associated epithelium. Eur J Pharm Sci 25(4–5):455–465.

Dobrovolskaia MA, Patri AK, Zheng J, Clogston JD, Ayub N, Aggarwal P, Neun BW, Hall JB, McNeil SE. 2009. Interaction of colloidal gold nanoparticles with human blood: Effects on particle size and analysis of plasma protein binding profiles. Nanomedicine 5(2):106–117.

Doyle-McCullough M, Smyth SH, Moyes SM, Carr KE. 2007. Factors influencing intestinal microparticle uptake in vivo. Int J Pharm 335(1–2):79–89.

Florence AT, Hillery AM, Hussain N, Jani PU. 1995. Factors affecting the oral uptake and translocation of polystyrene nanoparticles: Histological and analytical evidence. J Drug Target 3(1):65–70.

Florence AT. 2007. Pharmaceutical nanotechnology: More than size. Ten topics for research. Int J Pharm 339(1–2):1–2.

Florence AT, Sakthivel T, Toth I. 2000. Oral uptake and translocation of a polylysine dendrimer with a lipid surface. J Control Release 65(1–2):253–259.

Gebert A, Rothkotter HJ, Pabst R. 1996. M cells in Peyer's patches of the intestine. Int Rev Cytol 167:91–159.

Geiser M, Rothen-Rutishauser B, Kapp N, Schurch S, Kreyling W, Schulz H, Semmler M, Im HV, Heyder J, Gehr P. 2005. Ultrafine particles cross cellular membranes by nonphagocytic mechanisms in lungs and in cultured cells. Environ Health Perspect 113(11):1555–1560.

Hariharan S, Bhardwaj V, Bala I, Sitterberg J, Bakowsky U, Ravi Kumar MN. 2006. Design of estradiol loaded PLGA nanoparticulate formulations: A potential oral delivery system for hormone therapy. Pharm Res 23(1):184–195.

He C, Hu Y, Yin L, Tang C, Yin C. 2010. Effects of particle size and surface charge on cellular uptake and biodistribution of polymeric nanoparticles. Biomaterials 31(13):3657–3666.

Hillery AM, Jani PU, Florence AT. 1994. Comparative, quantitative study of lymphoid and non-lymphoid uptake of 60 nm polystyrene particles. J Drug Target 2(2):151–156.

Hillyer JF, Albrecht RM. 2001. Gastrointestinal persorption and tissue distribution of differently sized colloidal gold nanoparticles. J Pharm Sci 90(12):1927–1936.

Hirn S, Semmler-Behnke M, Schleh C, Wenk A, Lipka J, Schäffler M, Takenaka S, Möller W, Schmid G, Simon U, Kreyling WG. Particle size-dependent and surface charge-dependent biodistribution of gold nanoparticles after intravenous administration. Eur J Pharm Biopharm. 2010 Dec 31. [Epub ahead of print]

Hussain N, Florence AT. 1998. Utilizing bacterial mechanisms of epithelial cell entry: Invasin-induced oral uptake of latex nanoparticles. Pharm Res 15(1):153–156.

Jani P, Halbert GW, Langridge J, Florence AT. 1990. Nanoparticle uptake by the rat gastrointestinal mucosa: Quantitation and particle size dependency. J Pharm Pharmacol 42(12): 821–826.

Jani P, Halbert GW, Langridge J, Florence AT. 1989. The uptake and translocation of latex nanospheres and microspheres after oral administration to rats. J Pharm Pharmacol 41(12):809–812.

Jani PU, Nomura T, Yamashita F, Takakura Y, Florence AT, Hashida M. 1996. Biliary excretion of polystyrene microspheres with covalently linked FITC fluorescence after oral and parenteral administration to male Wistar rats. J Drug Target 4(2):87–93.

Kuo CT, Yu JY, Huang MJ, Chen CH. 2010. On the size evolution of gold-monolayer-protected clusters by ligand place-exchange reactions: the effect of headgroup-gold interactions. Langmuir 26(9):6149–6153.

Lacerda SH, Park JJ, Meuse C, Pristinski D, Becker ML, Karim A, Douglas JF. 2010. Interaction of gold nanoparticles with common human blood proteins. ACS Nano 4(1):365–379.

Lundqvist M, Stigler J, Elia G, Lynch I, Cedervall T, Dawson KA. 2008. Nanoparticle size and surface properties determine the protein corona with possible implications for biological impacts. Proc Natl Acad Sci USA 105(38): 14265–14270.

Lundqvist M, Sethson I, Jonsson BH. 2004. Protein adsorption onto silica nanoparticles: Conformational changes depend on the particles' curvature and the protein stability. Langmuir 20(24):10639–10647.

Nassimi M, Schleh C, Lauenstein HD, Hussein R, Hoymann HG, Koch W, Pohlmann G, Krug N, Sewald K, Rittinghausen S, Braun A, Muller-Goymann C. 2010. A toxicological evaluation of inhaled solid lipid nanoparticles used as a potential drug delivery system for the lung. Eur J Pharm Biopharm 75(2):107–116.

Nassimi M, Schleh C, Lauenstein HD, Hussein R, Lubbers K, Pohlmann G, Switalla S, Sewald K, Muller M, Krug N, Muller-Goymann CC, Braun A. 2009. Low cytotoxicity of solid lipid nanoparticles in in vitro and ex vivo lung models. Inhal Toxicol 21(S1):104–109.

Oeff K, Konig A. 1955. Das Blutvolumen einiger Rattenorgane und ihre Restblutmenge nach entbluten bzw. durchspülung - Bestimmung mit P-32-markierten Erythrocyten. Naunyn-Schmiedebergs Archiv Fur Experimentelle Pathologie Und Pharmakologi 226(1):98–102.

Pan Y, Leifert A, Ruau D, Neuss S, Bornemann J, Schmid G, Brandau W, Simon U, Jahnen-Dechent W. 2009. Gold nanoparticles of diameter 1.4 nm trigger necrosis by oxidative stress and mitochondrial damage. Small 5(18):2067–2076.

Pan Y, Neuss S, Leifert A, Fischler M, Wen F, Simon U, Schmid G, Brandau W, Jahnen-Dechent W. 2007. Size-dependent cytotoxicity of gold nanoparticles. Small 3(11):1941–1949.

Potten CS, Loeffler M. 1990. Stem cells: Attributes, cycles, spirals, pitfalls and uncertainties. Lessons for and from the crypt. Development 110(4):1001–1020.

Powell JJ, Faria N, Thomas-McKay E, Pele LC. 2010. Origin and fate of dietary nanoparticles and microparticles in the gastrointestinal tract. J Autoimmun 34(3):J226–233.

Rimoldi M, Rescigno M. 2005. Uptake and presentation of orally administered antigens. Vaccine 23(15):1793–1796.

Ruenraroengsak P, Cook JM, Florence AT. 2010. Nanosystem drug targeting: Facing up to complex realities. J Control Release 141(3):265–276.

Samstein RM, Perica K, Balderrama F, Look M, Fahmy TM. 2008. The use of deoxycholic acid to enhance the oral bioavailability of biodegradable nanoparticles. Biomaterials 29(6):703–708.

Sass W, Dreyer HP, Seifert J. 1990. Rapid insorption of small particles in the gut. Am J Gastroenterol 85(3):255–260.

Schmid G. 2008. The relevance of shape and size of Au55 clusters. Chem Soc Rev 37(9):1909–1930.

Seifert J, Sass W. 1990. Intestinal absorption of macromolecules and small particles. Dig Dis 8(3):169–178.

Seifert J, Haraszti B, Sass W. 1996. The influence of age and particle number on absorption of polystyrene particles from the rat gut. J Anat 189(Pt 3):483–486.

Semmler-Behnke M, Kreyling WG, Lipka J, Fertsch S, Wenk A, Takenaka S, Schmid G, Brandau W. 2008. Biodistribution of 1.4- and 18-nm gold particles in rats. Small 4(12): 2108–2111.

Shang W, Nuffer JH, Muniz-Papandrea VA, Colon W, Siegel RW, Dordick JS. 2009. Cytochrome C on silica nanoparticles: Influence of nanoparticle size on protein structure, stability, and activity. Small 5(4):470–476.

Smyth SH, Feldhaus S, Schumacher U, Carr KE. 2008. Uptake of inert microparticles in normal and immune deficient mice. Int J Pharm 346(1–2):109–118.

Sonavane G, Tomoda K, Sano A, Ohshima H, Terada H, Makino K. 2008. In vitro permeation of gold nanoparticles through rat skin and rat intestine: Effect of particle size. Colloids Surf B Biointerfaces 65(1):1–10.

Sperling RA, Rivera Gil P, Zhang F, Zanella M, Parak WJ. 2008. Biological applications of gold nanoparticles. Chem Soc Rev 37 (9):1896–1908.

Tominaga T, Tenma S, Watanabe H, Giebel U, Schmid G. 1996. Tracer diffusion of a ligand-stabilized two-shell gold cluster. Chem Lett (12):1033–1034.

Torjman MC, Joseph JI, Munsick C, Morishita M, Grunwald Z. 2005. Effects of isoflurane on gastrointestinal motility after brief exposure in rats. Int J Pharm 294(1–2):65–71.

Vertegel AA, Siegel RW, Dordick JS. 2004. Silica nanoparticle size influences the structure and enzymatic activity of adsorbed lysozyme. Langmuir 20(16):6800–6807.

Walczyk D, Bombelli FB, Monopoli MP, Lynch I, Dawson KA. 2010. What the cell 'sees' in bionanoscience. J Am Chem Soc 132(16):5761–5768.

6.3 Beitrag als Co-Autorin

Der Beitrag als Co-Autorin für die Publikation „Size and surface charge of gold nanoparticles determine absorption across intestinal barriers and accumulation in secondary target organs after oral administration" bestand hauptsächlich in der experimentellen Durchführung und weiterhin in der Auswertung der erhobenen Daten. Für jedes Tier wurde die gemessene Radioaktivität mit der korrespondierenden Gold-Nanopartikel-Masse korreliert. Somit konnte der prozentuale Anteil der zu Beginn applizierten Gold-Nanopartikel für das jeweilige Organ/Gewebe berechnet werden, woraus sich das Verteilungsmuster der Gold-Nanopartikel im Körper ergab. Anschließend wurde eine statistische Analyse (Oneway ANOVA mit post hoc Tukey bzw. Student's t-Test) durchgeführt.

7 Danksagung

8 Curriculum Vitae

9 Eidesstattliche Versicherung

Hirn, Stephanie
Name, Vorname

Ich erkläre hiermit an Eides statt,
dass ich die vorliegende Dissertation mit dem Thema:

Biodistribution von Gold-Nanopartikeln in Abhängigkeit von ihrer Größe, Oberflächenladung und Applikationsart

selbständig verfasst, mich außer der angegebenen keiner weiteren Hilfsmittel bedient und alle Erkenntnisse, die aus dem Schrifttum ganz oder annähernd übernommen sind, als solche kenntlich gemacht und nach ihrer Herkunft unter Bezeichnung der Fundstelle einzeln nachgewiesen habe.
Ich erkläre des Weiteren, dass die hier vorgelegte Dissertation nicht in gleicher oder in ähnlicher Form bei einer anderen Stelle zur Erlangung eines akademischen Grades eingereicht wurde.

Ort, Datum

Unterschrift Doktorandin